Article

# Synthesis, Photophysical Properties, Theoretical Studies, and Living Cancer Cell Imaging Applications of New 7-(Diethylamino)quinolone Chalcones

Daniel Insuasty,* Mario Mutis, Jorge Trilleras, Luis A. Illicachi, Juan D. Rodríguez, Andrea Ramos-Hernández, Homero G. San-Juan-Vergara, Christian Cadena-Cruz, José R. Mora, José L. Paz, Maximiliano Méndez-López, Edwin G. Pérez, Margarita E. Aliaga, Jhesua Valencia, and Edgar Márquez

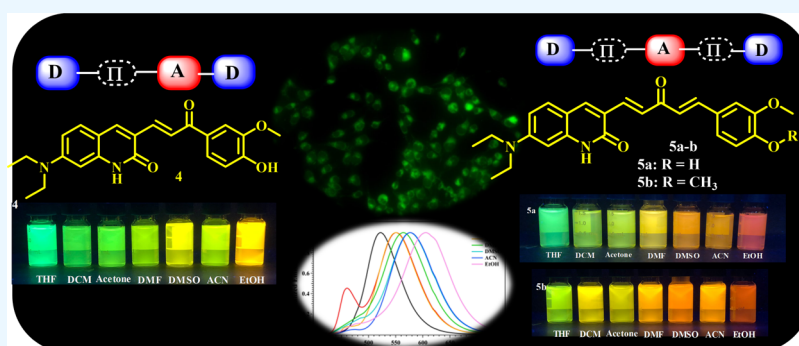Cite This: *ACS Omega* 2024, 9, 18786−18800

Read Online

ACCESS | Metrics & More | Article Recommendations | SI Supporting Information

**ABSTRACT:** In this article, three unsymmetrical 7-(diethylamino)quinolone chalcones with D-$\pi$−A-D and D-$\pi$−A-$\pi$-D type push−pull molecular arrangements were synthesized via a Claisen−Schmidt reaction. Using 7-(diethylamino)quinolone and vanillin as electron donor (D) moieties, these were linked together through the $\alpha,\beta$-unsaturated carbonyl system acting as a linker and an electron acceptor (A). The photophysical properties were studied, revealing significant Stokes shifts and strong solvatofluorochromism caused by the ICT and TICT behavior produced by the push−pull effect. Moreover, quenching caused by the population of the TICT state in THF−$H_2O$ mixtures was observed, and the emission in the solid state evidenced a red shift compared to the emission in solution. These findings were corroborated by density functional theory (DFT) calculations employing the wb97xd/6-311G(d,p) method. The cytotoxic activity of the synthesized compounds was assessed on BHK-21, PC3, and LNCaP cell lines, revealing moderate activity across all compounds. Notably, compound **5b** exhibited the highest activity against LNCaP cells, with an $LC_{50}$ value of 10.89 $\mu$M. Furthermore, the compounds were evaluated for their potential as imaging agents in living prostate cells. The results demonstrated their favorable cell permeability and strong emission at 488 nm, positioning them as promising candidates for cancer cell imaging applications.

## 1. INTRODUCTION

In recent decades, organic small molecular dyes have gained great research value due to their low cost of production as well as their ease of synthesis from commercial materials and their possibility of modifications. Moreover, these molecules usually display a broad spectrum of applications, such as optoelectronic devices,[1] dye-sensitized solar cells,[2] nonlinear optical properties (NLO), molecular probes,[3] biological properties,[4] and sensors.[5] Furthermore, fluorescent compounds are important tools in biomedical imaging due to their ability to selectively bind to specific targets within biological systems and emit light upon excitation.[6] This property allows researchers to track the movement of molecules, monitor cellular activity, and visualize the progression of diseases. Currently, advances in

fluorescence imaging technology have led to significant improvements in the sensitivity and resolution of biological imaging,[7] enabling researchers to study biological systems with unprecedented detail. Therefore, the development of new and improved fluorescent compounds is crucial for the continued advancement of biomedical imaging, as well as the diagnosis and treatment of various diseases.[8]

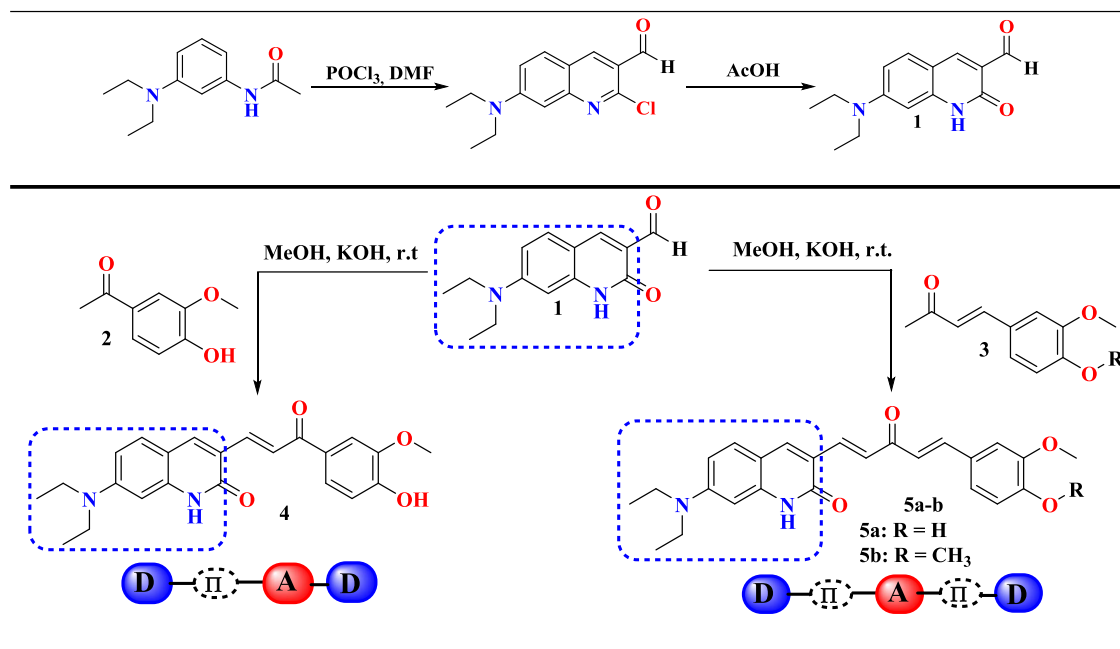**Scheme 1. Synthesis of New 7-(diethylamino)quinolone Chalcones**



In this regard, great effort has been made in developing new fluorophores with improved properties from classical scaffolds, the majority of these are created through structural alterations of a small number of classical "core" dyes,[9] including naphthalimide,[10] coumarin,[11] BODIPY,[6] fluorescein,[12] and rhodamine.[13] However, the creation of new "core" fluorophores could provide greater versatility and flexibility for developing novel fluorescent probes with unique properties. In this context, quinolones have been of great interest due to their excellent photochemical stability (laser irradiation), favorable biocompatibility,[14] excellent mechanical properties,[15] synthetic versatility,[16] and good thermal stability.[17] Even more the relevance of the incorporation of dialkylamino groups in the quinolone moiety has been assessed on its key effect on the photophysical properties,[18] such as UV–vis spectra (causing a red shift), Stokes shift, and fluorescence quantum yield, generating high efficient materials in the electron transport, high photoluminescence efficiencies, and biological imaging properties.[19] In addition, quinolones have exhibited interesting biological properties, such as antimicrobial,[20] antifungal,[21] antiviral,[22] antimalarial,[23] antituberculosis,[24] antioxidant,[25] and anticancer.[26]

On the other hand, chalcones are a class of organic compounds that contain a central $\alpha,\beta$-unsaturated carbonyl system, which has attracted significant attention,[27] due to their diverse applications in the fields of medicine,[26] material science, and optics.[28] Moreover, the chalcones due to the $\pi$-conjugated system and the two aromatic rings that act as donors and acceptors provide a reasonable fluorescence quantum yield,[27] efficient stabilization of charge-transfer processes in the excited state,[28] long-wavelength emission ($\lambda_{em}$), and large Stokes shifts,[29] which means that they have potential applications in fluorescence microscopy or bioimaging applications as they can improve image sensitivity by reducing the interference caused by self-absorption or autofluorescence.[30−32]

This study focuses on the design, synthesis, and investigation of the photophysical properties of three unsymmetrical 7-(diethylamino)quinolone chalcones. These chalcones contain electron-rich 7-(diethylamino)quinolone and vanillin moieties acting as electron donors (D), linked together through an $\alpha,\beta$-unsaturated carbonyl system acting as a linker and an acceptor (A), resulting in D-$\pi$−A-D and D-$\pi$−A-$\pi$-D type push−pull molecular arrangements. Additionally, we evaluated the cell viability and toxicity in a normal cell line (BHK-21) and two prostate cancer cell lines (LNCaP and PC3). Furthermore, fluorescence imaging was carried out to evaluate their potential in bioimaging applications.

## 2. RESULTS AND DISCUSSION

**2.1. Synthesis.** The detailed synthetic routes for 7-(diethylamino)quinolone chalcones **4a** and **5a−b** derivatives are outlined in Scheme 1. Target chromophores were readily synthesized following the literature method through a one-step Claisen−Schmidt condensation reaction between equimolar amounts of 7-(diethylamino)-2-oxo-quinolinaldehyde **1** and ketones **2** and **3a−b**.[33] The reaction was carried out in methanol and KOH at room temperature for 36 h; after completion, it was neutralized with HCl, and the resulting precipitate was collected by filtration and washed with MeOH/H$_2$O, leading to the isolation of the expected target compounds **4a** and **5a−b** with yields between 58 and 73%. The noncommercial 7-(diethylamino)-2-oxo-quinolinaldehyde **1** was prepared in two steps. Initially, by a Meth−Cohn reaction from N-(3-(diethylamino)phenyl)acetamide, 2-chloro-7-(diethylamino)quinoline-3-carbaldehyde was obtained, followed by hydrolysis with acetic acid (70%). The structures of the new chromophores, 7-(diethylamino)-quinolone chalcones **4a** and **5a−b**, were ascertained by FTIR, $^1$H NMR, and $^{13}$C NMR (in DMSO-$d_6$), and mass spectrometric analysis is summarized in the Experimental Section. The $^1$H NMR spectrum of the compound **5b** showed four doublets at 7.74, 7.68 ppm ($J$ = 15.7 Hz) and 7.62, 7.21 ($J$ = 15.9 Hz) assigned to protons of the $\alpha,\beta$-unsaturated moiety, confirming the condensation between **1** and **3b**, as well as $E$ configuration of the new double bonds formed. In the $^{13}$C

**Table 1. Spectroscopic Properties of Fluorophores 4, 5a, and 5b at 5.0 $\mu$M**

| compounds | 4 | | | 5a | | | 5b | | |
|---|---|---|---|---|---|---|---|---|---|
| solvent | Abs, nm ($\varepsilon$, M$^{-1}$cm$^{-1}$) | Em[b], nm ($\varphi$)[a] | Stokes shift, cm$^{-1}$ | Abs, nm ($\varepsilon$, M$^{-1}$cm$^{-1}$) | Em, nm ($\varphi$)[a] | Stokes shift, cm$^{-1}$ | Abs, nm ($\varepsilon$, M$^{-1}$cm$^{-1}$) | Em, nm ($\varphi$)[a] | Stokes shift, cm$^{-1}$ |
| THF | 437 (38 080) | 502 | 2963 | 434 (69 500) | 523 (0.33) | 3921 | 443 (28 840) | 525 (0.49) | 3226 |
| DCM | 443 (23 820) | 521 (0.66) | 3380 | 452 (35 160) | 552 (0.63) | 4008 | 457 (39 480) | 552 (0.63) | 3766 |
| acetone | 440 (39 020) | 521 (0.73) | 3533 | 452 (21 000) | 550 | 3942 | 445 (37 900) | 552 (0.35) | 4356 |
| DMF | 448 (21 740) | 534 (0.31) | 3489 | 456 (32 680) | 564 (0.46) | 4199 | 459 (32 340) | 569 (0.42) | 4212 |
| DMSO | 454 (32 580) | 543 (0.53) | 3610 | 463 (32 180) | 576 (0.44) | 4237 | 465 (17 420) | 581 (0.37) | 4294 |
| ACN | 441 (60 960) | 539 (0.79) | 4123 | 448 (26 380) | 577 (0.47) | 4990 | 455 (44 600) | 579 (0.33) | 4611 |
| EtOH | 443 (46 000) | 565 (0.43) | 4811 | 459 (34 880) | 606 (0.14) | 5284 | 462 (31 060) | 604 (0.10) | 5089 |

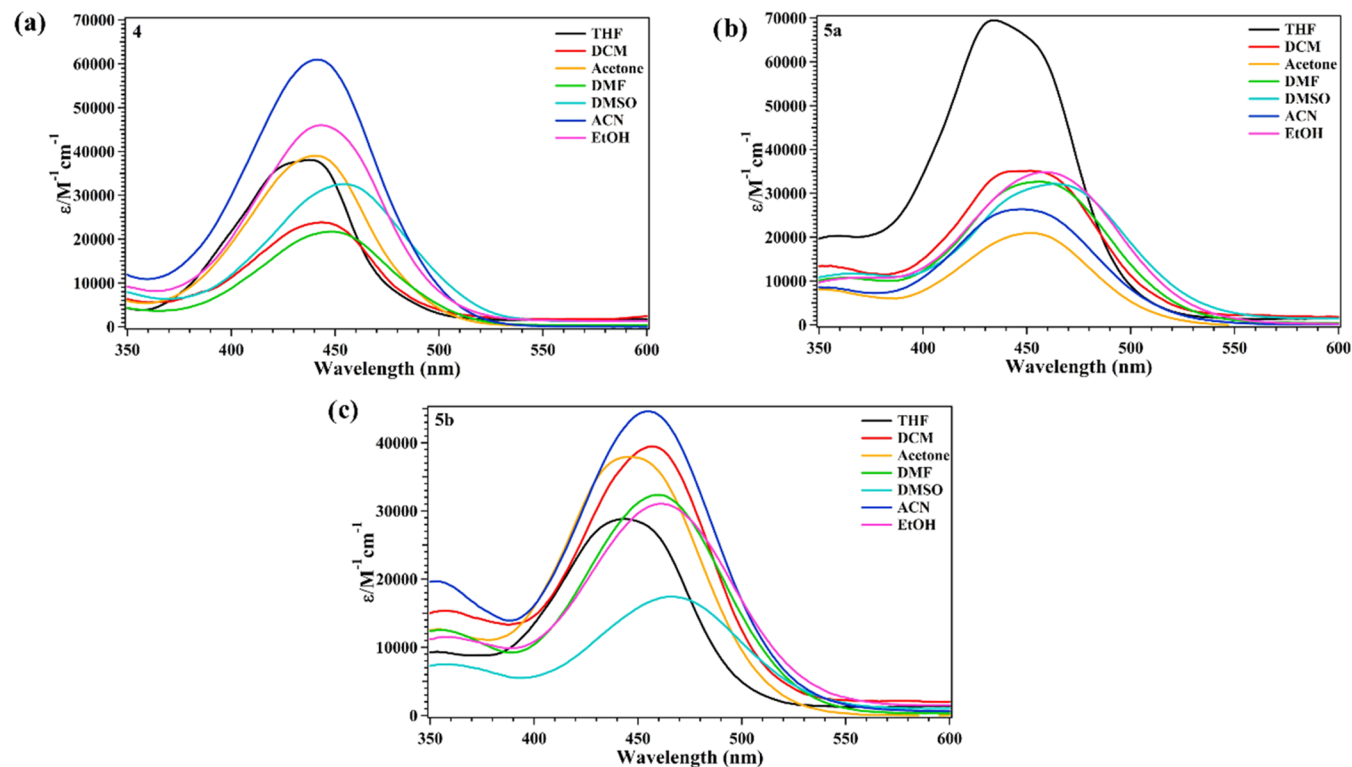[a]Relative quantum yield using Rhodamine B as standard. [b]The measures were made at 2.0 $\mu$M.



**Figure 1.** Absorption spectra of (a) **4**, (b) **5a**, and (c) **5b** (5.0 $\mu$M) in different solvents.

NMR spectrum, the total expected signals (i.e., 24) for compound **5b** were observed (see the Supporting Information).

**2.2. Photophysical Properties.** The optical properties of **4**, **5a**, and **5b** were determined by recording the UV−vis absorption and fluorescence emission spectra in seven different solvents (THF, DCM, acetone, DMF, DMSO, ACN, and EtOH) as outlined in Table 1. The UV−vis spectra (Figure 1) showed an intense absorption maximum centered in the region of 434−465 nm, which could be assigned to an intramolecular charge transfer (ICT) process from the diethylamino and vanillin moieties to the acceptor segments.[15,34] The nature of the solvent had a considerable effect on the UV−vis absorption properties of the three compounds, suggesting that the difference in the dipole moment between the equilibrium ground state and the Franck−Condon excited state is large.[35] For example, the maximum absorption of **5a** shifted from 434 nm in THF to 463 nm in DMSO (Table 1). The intense red shift of the $\lambda_{max}$ values indicates electronic transitions with ICT character, which can also be verified by the molar absorption

coefficient magnitude for all of the dyes[36] ($\varepsilon$ = 1.7 × 10$^4$−6.9 × 10$^4$ M$^{-1}$ cm$^{-1}$). Theoretical calculations were performed at the time-dependent wb97xd/6-311g (d,p) level in THF to determine the nature of the electronic transitions that gave rise to the experimental absorption bands. The intense absorption band experimentally registered in the 434−465 nm region is due to the transition to the lowest-lying singlet excited state S$_1$ predicted with a considerable oscillator strength ($f$ = 1.63, 2.01, and 1.92 for **4**, **5a**, and **5b**, respectively). This transition is depicted by the HOMO → LUMO monoexcitation in all of the dyes.

The fluorescence emission spectra of compounds **4**, **5a**, and **5b** (Figure 2) exhibited various emission profiles, which have a stronger dependence on the solvent environment than the absorption spectra, presenting structure bands with maximum emission in the 502−606 nm region. Interestingly, these compounds exhibited broad Stokes shifts (**4** 2963−4811, **5a** 3921−5284, and **5b** 3226−5089 cm$^{-1}$) in different solvents, indicating a fast relaxation from the excited state to lower energy vibrational states, which is beneficial for fluorescence
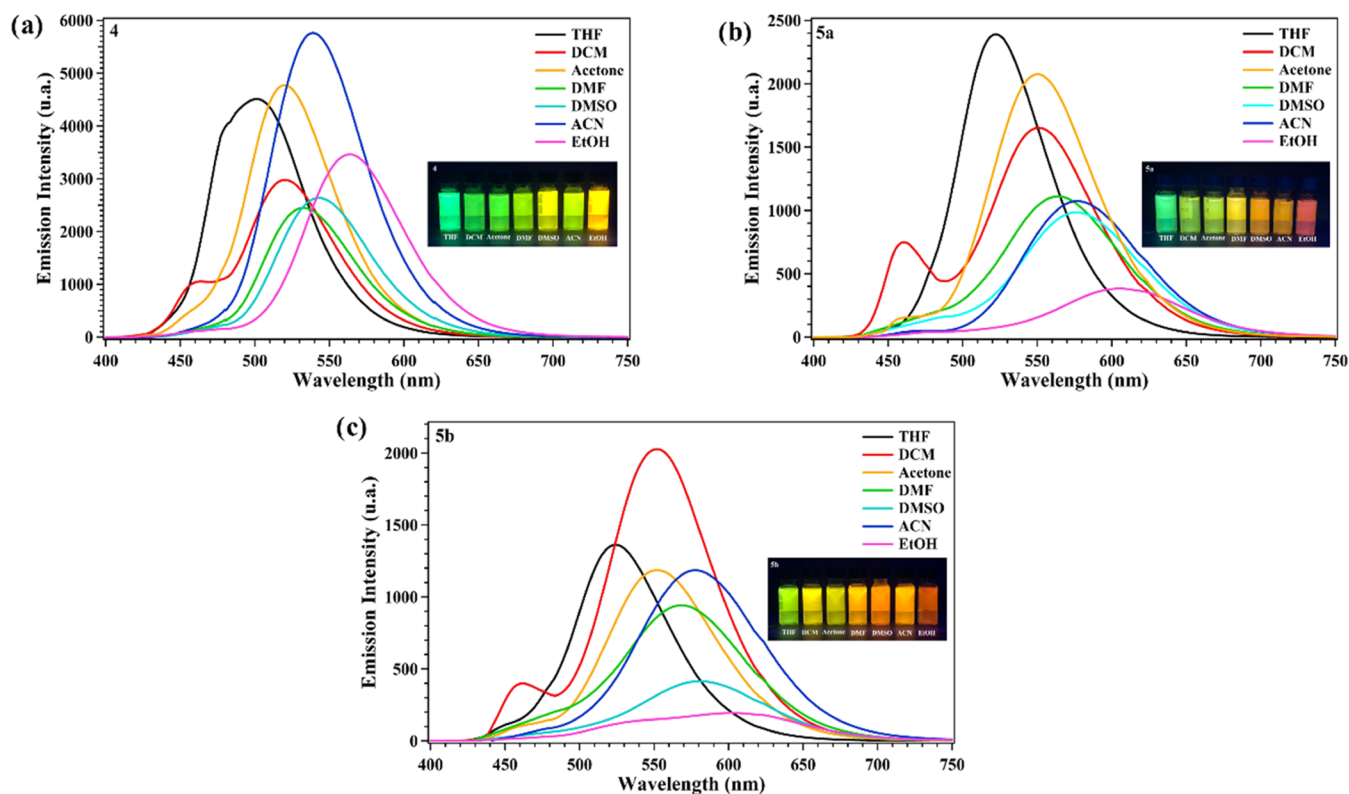
**Figure 2.** Emission spectra of (a) **4**, (b) **5a**, and (c) **5b** in different solvents. Pictures of solutions under UV light (365 nm lamp) in solvents with increasing polarity.
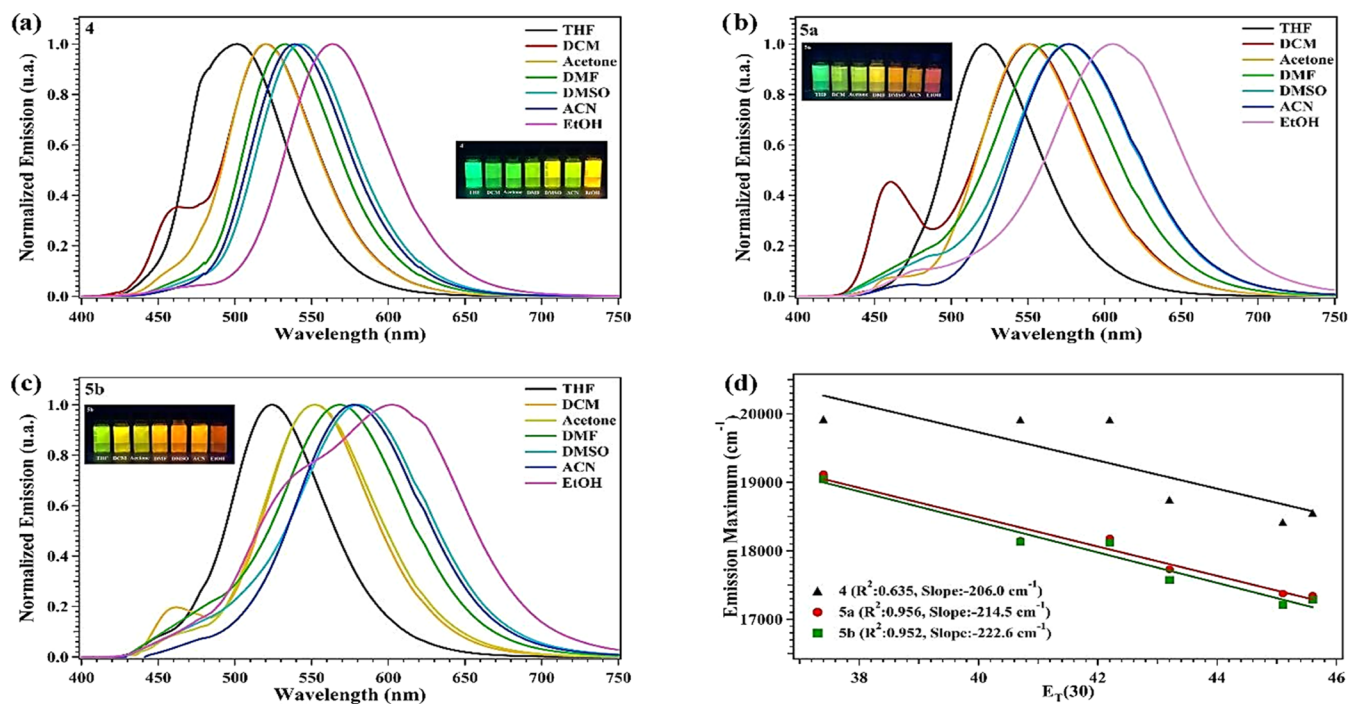


**Figure 3.** Emission spectra of fluorophores (a) **4**, (b) **5a**, and (c) **5b** in different solvents at 25 °C. Pictures of solutions under UV light (365 nm lamp) in solvents of increasing polarity. (d) Plot of emission maximum vs $E_T(30)$ in aprotic solvents.

imaging.[37] As the solvent polarity increased from THF to ethanol, the emission peaks of **4**, **5a**, and **5b** displayed a red-shifted tendency from 502 to 563 nm, 523 to 606 nm, and 525 to 604 nm, respectively, showing a considerable bathochromic effect. These observations indicate that the excited state is

highly polar compared to the ground state, resulting in a stronger interaction of polar solvents in the excited state. The decrease in fluorescence intensity, along with the change in emission maximum, can be attributed to the significant impact of the twisted intramolecular charge transfer (TICT) effect in
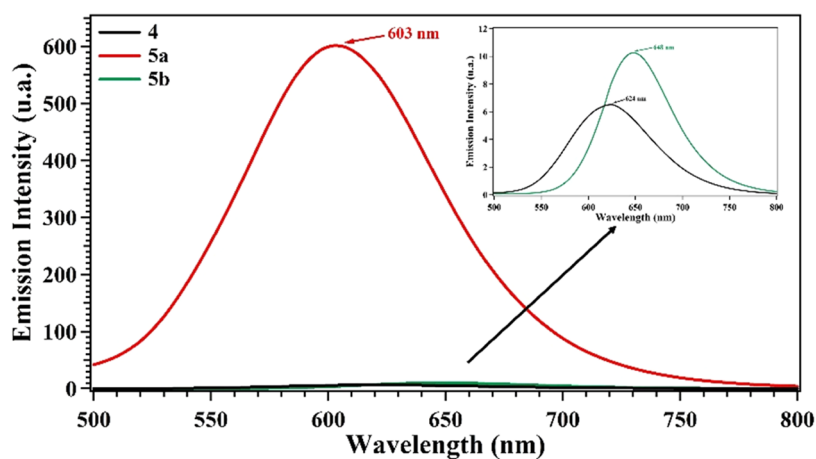
**Figure 4.** Solid-state emission spectra of compounds **4**, **5a**, and **5b**.

polar solvents.[38,39] The observed shift toward red in the emission intensity of fluorophores is attributed to the TICT process due to its susceptibility to different nonradiative decay processes. Unexpectedly, all of the compounds showed a dual emission in DCM, which could be attributed to an excited state proton transfer (ESPT) from DCM to the amide group of the chromophores caused by the photodegradation of DCM in the presence of UV−vis radiation.[40,41] Moreover, the optical band gap ($E^{0-0}$) was estimated from the interception of the absorption and emission bands for all of the compounds, resulting in values of 2.67, 2.56, and 2.55 eV for **4**, **5a**, and **5b**, respectively, exhibiting the same tendency as the calculated energy gap in THF.

**2.3. Solvatofluorochromism.** Preliminary studies to view the solvatofluorochromism effects were performed by checking the color change of **4**, **5a**, and **5b** in solutions of solvents with different polarities. All compounds displayed color changes from green in a moderate- polar solvent (THF) to red in a high polar solvent (EtOH; Figure 3). The significant difference in Stokes shift observed for compounds **4**, **5a**, and **5b** motivated us to investigate the charge transfer interaction more extensively. This was accomplished by examining the emission characteristics of the fluorophores in solvents of different polarities. The emission spectra showed positive solvatochromism properties with increasing solvent polarity because the highly polar TICT state is specially stabilized concerning a planar local excited (LE) state in polar solvents.[38,42] This positive solvatochromic behavior was quantitatively determined using different solvent polarity plots, such as the plot of the maximum emission band regarding the empirical polarity scale $E_T(30)$[43−45] as well as the plot of the relationship between Stokes shifts vs orientation polarizability (Lippert−Mataga plot).[29,46] The plot of emission maximum vs $E_T(30)$ (Figure 3d) displays a linear tendency of **4**, **5a**, and **5b** with negative slopes of −206.0 cm$^{-1}$ ($R^2 = 0.63$), − 214.5 cm$^{-1}$ ($R^2 = 0.96$), and −222.6 cm$^{-1}$ ($R^2 = 0.95$), respectively (Figure 3d). Nevertheless, compounds **5a** and **5b** showed many sheer slopes with linear coefficients better than those of **4**, evidencing a more significant variation of the solvatofluorochromism effect with the variation of solvent properties. These features confirm the assignment of this band to an ICT and TICT process produced by the push−pull effect into the D-$\pi$−A-D and D-$\pi$−A-$\pi$-D structures.[47] On the other hand, the Lippert−Mataga plot (Figure S2a) shows a low linearity tendency; this behavior can be due to specific solvent effects like preferential solvation,

hydrogen bonding, and charge-transfer interactions, which are produced by one or a few neighboring molecules and are determined by the specific chemical properties of both the fluorophore and the solvent.[48] The spectral offsets caused by the formation of ICT and TICT states are not explained by the Lippert−Mataga equation, because the feature of the ICT and TICT emission depends on the electron-donating and electron-accepting properties of groups within or linked to the fluorophore instead of polarity. In order to establish a connection between the observed solvatochromic shift in a positive direction and the twisted intramolecular charge transfer (TICT) phenomenon, we studied the Rettig plots (Figure S2b). The Rettig plots for compounds **4**, **5a**, and **5b** revealed a linear relationship between the Stokes shift and the solvent polarity parameter $\Delta f$, indicating that the primary state in which TICT occurs is the initial single state. Consequently, the linear association observed in the Rettig plots suggests the coexistence of both TICT and ICT within these fluorophores.[49,50]

**2.4. Solid-State Emission in Powder.** The solid-state fluorescence spectra were registered at room temperature and exhibited emission bands centered at 624, 603, and 648 nm for **4**, **4a**, and **5b**, respectively (Figure 4). Compound **5a** showed a blue shift compared to **4** and **5b** by the −OH group in the 4-position $\pi$-extended vanillin moiety, indicating the existence of a twisted arrangement in the solid form.[51] In addition, the insertion of the electron-donating group −OCH$_3$ (**5b**) instead of −OH (**5a**) caused an increase in the donor ability of vanillin, leading to enhanced D−A interactions. However, compound **5a** exhibits a broad and intense band caused by the highly conjugated system.[52] On the other hand, the solid-state emission spectra are similar to those acquired in a highly polar solvent such as ethanol. Conversely, an opposite behavior was found in **4** and **5b**, showing a red shift compared to those in solution, indicating the existence of intermolecular $\pi$−$\pi$ interactions in the solid state.[52,53] The results suggest that changing the molecular structure makes it possible to control the fluorescence properties, such as fluorescence intensity, emission band offset, and intermolecular interaction in the solid state.

**2.5. Acid−Base Responsive Emission.** To investigate the acid−base response on the emission behavior of **4**, **5a**, and **5b**, emission spectra in THF with TFA and TEA equivalents were recorded (Figure S3). In all cases, the emission spectra show a blue shift (negative acidocromism) with a gradually decreasing
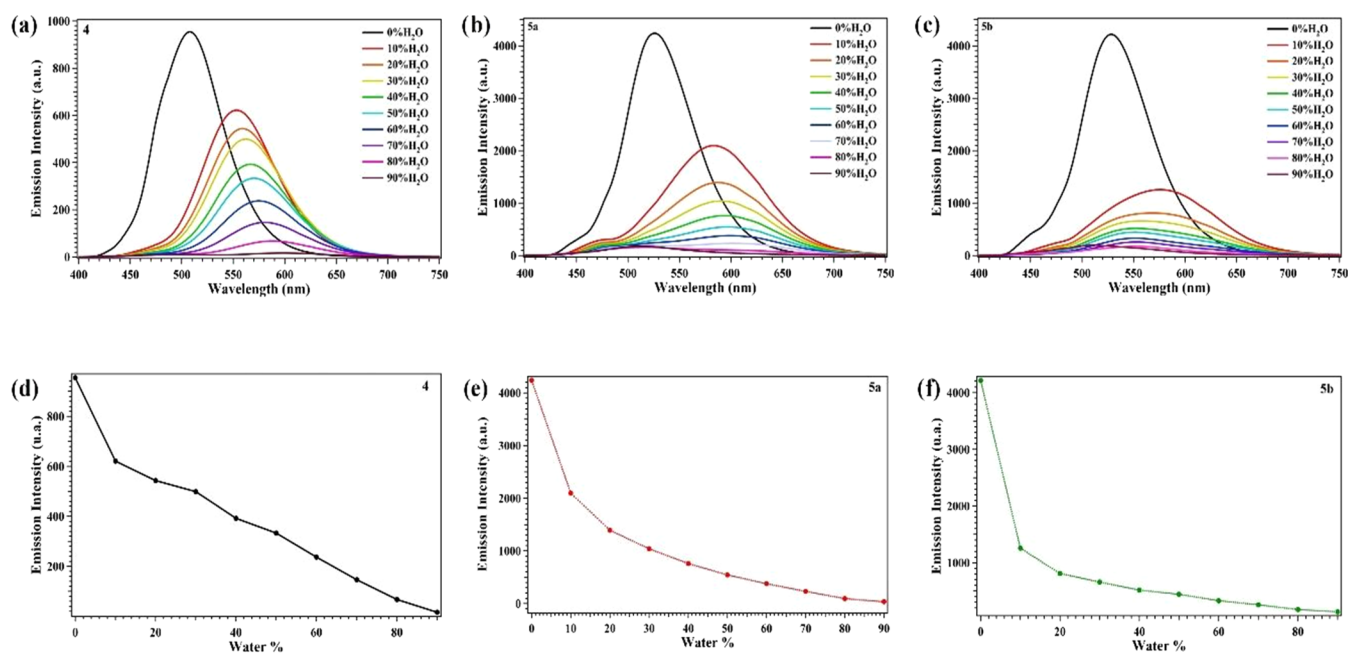
**Figure 5.** Emission spectra of (a) **4**, (b) **5a**, and (c) **5b** in THF/water and (d)−(f) plot between emission intensity vs fraction of water ($f_W$) in THF/water.
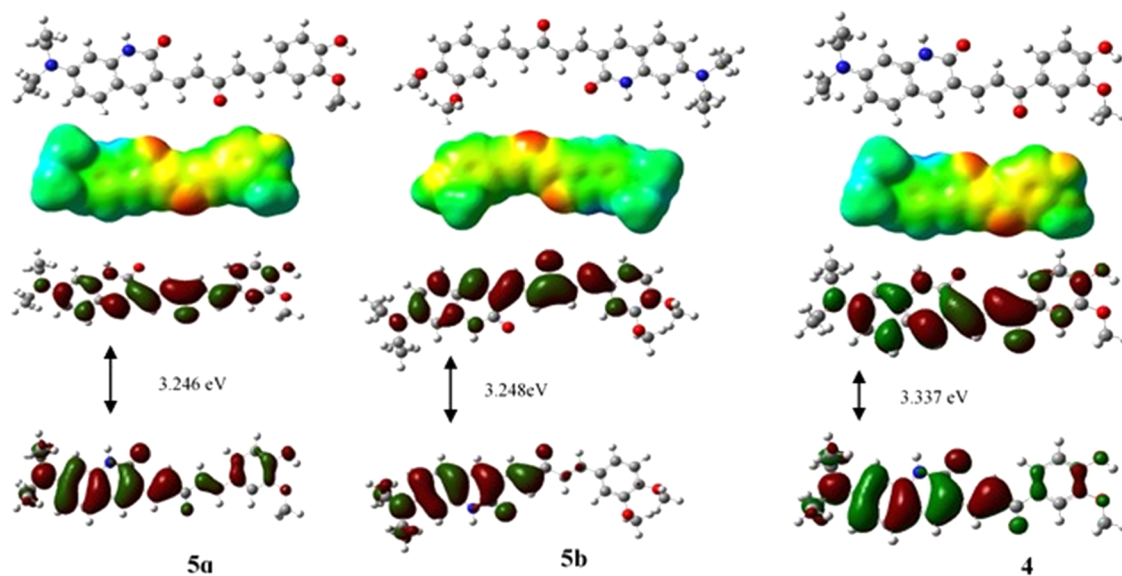


**Figure 6.** Optimized structures, SEP, and frontier orbitals for **5a**, **5b**, and **4** obtained at the Wb97xd/6-311g(d,p) level of theory.

emission peak, which could be attributed to the protonation of nitrogen at the *N,N*-diethylamino terminal group.[54] On the other hand, the addition of TEA caused similar results to the TFA titration with a negative acidocromism, and the emission intensity decreased due to the deprotonation of the −OH group of the phenol moiety. However, compound **5b** does not show this trend due to the absence of this group, which is replaced by a methoxy group.

**2.6. Aggregation Properties.** To investigate the effects of aggregation on the emission performance, emission spectra of **4**, **5a**, and **5b** were recorded in different THF−water mixtures (from 0 to 90%; Figure 5). In all dyes, the emission displayed a fluorescence quenching with a red shift upon increasing amounts of water ($f_W$) attributed to the influence of the TICT effect. In the TICT state, an *N,N*-diethylamino donor

undergoes a torsional motion of around 90° when exposed to light, creating a chemically active species that does not emit light.[55−57] Molecules exhibiting TICT characteristics are consistently identified by their substantial molecular dipoles and a distinct uneven distribution of electrons in emission-related frontier molecular orbitals. These characteristics are confirmed by theoretical calculation results. Figure 6 shows that in the HOMO level, the electron cloud is primarily concentrated on the *N,N*-diethylamino unit, while in the LUMO level, it is predominantly situated on the quinolone unit.[58] On the other hand, all compounds could be candidates for determining water content in organic solvents acting as fluorescent sensors.[59]

**2.7. Theoretical Calculations.** The minimum energy structures of all of the compounds were confirmed through

**Table 2. Variation of Some Specific Bonds in the Ground and First Excited States in THF Using the wb97xd/6-311g(d,p) Level of Theory and CPCM Approximation**

| compounds | $N_1$-$C_2$ | $C_3$-$C_4$ | $C_4$-$C_5$ | $C_5$-$C_6$ | $C_6$-$O_7$ | $C_9$-$O_{10}$ | $C_{11}$-$O_{12}$ | $\mu$(D) |
|---|---|---|---|---|---|---|---|---|
| **5a** | 1.37667 | 1.45386 | 1.33958 | 1.48395 | 1.21983 | 1.36463 | 1.34961 | 6.9220 |
| **5a**[a] | 1.3745 | 1.44542 | 1.36261 | 1.42571 | 1.29330 | 1.36539 | 1.35172 | 6.9968 |
| **5b** | 1.3741 | 1.45358 | 1.33973| | 1.48313 | 1.21900 | 1.36561 | 1.36854 | 7.7461 |
| **5b**[a] | 1.37607 | 1.44560 | 1.36154 | 1.42706 | 1.29189 | 1.36750 | 1.36901 | 8.1422 |
| **4** | 1.37421 | 1.45471 | 1.33943 | 1.48329 | 1.21952 | 1.36463 | 1.34826 | 7.6802 |
| **4**[a] | 1.37003 | 1.41086 | 1.37636 | 1.45583 | 1.234387 | 1.36531 | 1.3497 | 9.1999 |

[a]indicates first excitation state. Bond longitude in Anstrong.

**Table 3. Excitation Energy, Wavelength, and Oscillator Strength Obtained from DFT Calculations in THF**

| molecule | excited state | transition | excitation energy (eV) | wavelength | oscillator strength |
|---|---|---|---|---|---|
| **5a** | 1 | HOMO−LUMO | 3.2458 | 381.99 | 2.0051 |
| | 2 | HOMO(−1)−LUMO | 3.9252 | 315.87 | 0.2447 |
| | 3 | HOMO(−2)−LUMO(+2) | 5.7780 | 214.58 | 0.7702 |
| **5b** | 1 | HOMO−LUMO | 3.2479 | 381.74 | 1.9161 |
| | 2 | HOMO(−1)−LUMO | 4.1031 | 302.17 | 0.3836 |
| | 3 | HOMO(−2)−LUMO(+2) | 5.7673 | 214.98 | 0.7751 |
| **4** | 1 | HOMO−LUMO | 3.3366 | 371.59 | 1.6313 |
| | 2 | HOMO(−1)−LUMO | 4.2715 | 290.26 | 0.1114 |
| | 3 | HOMO(−2)−LUMO(+2) | 5.8139 | 213.26 | 0.9813 |

frequency calculations, ensuring that no imaginary frequencies were generated. Figure 6 displays the structures with minimum energy; additionally, the uppermost part of this figure shows a 2D structure based on the studied compound with specific atoms arbitrarily labeled to facilitate comprehension of the electron flux within the D-$\pi$−A-$\pi$-D system. In this sense, a discussion of the geometry obtained through optimization is initially performed, followed by a discussion of how frontier orbitals affect the absorption and emission processes.

Table 2 shows the variation of some important bonds as well as the dipolar momentum ($\mu$) in both the ground and the first excited state in THF solvent. Notably, except for the bonds between $C_9$−$O_{10}$ and $C_{11}$−$O_{12}$, all selected bonds exhibit a shorter length in the excited state than in the ground state. This observation supports the hypothesis mentioned above that the studied compounds demonstrate an intricate charge transfer toward the carbonyl moiety, coupled with the $\pi$−$\pi$* transition serving as the initial transition; in other words, this result suggests that an efficient electronic conjugation between D and A takes place. Conversely, the bonds denoted as $C_9$−$O_{10}$ and $C_{11}$−$O_{12}$ exhibit a contrary trend as they display a greater length in the excited state. This finding strongly indicates that, in both the O−H and O−$CH_3$ groups, the inductive effect predominates over the resonance effect, and they have not increased the electronic density over the aromatic ring. In addition, a close inspection of both bonds shows the probability of hydrogen bond formation due to the proximity of these two bonds; consequently, the potential formation of a hydrogen bond could reduce the electron density of the oxygen atoms and the donor effect via resonance.

Another essential factor that can be observed in Table 2 is the increase of the dipole momentum on going from the ground state to the first excited state. These findings are consistent with the experimental bathochromic shift observed in the absorption spectra of all studied compounds as the polarity of the solvent increases. In such scenarios, the relaxed excited state S1 is more energetically stable than the ground state S0, leading to a significant red shift in the absorption spectra.[60]

The shape of its frontier orbitals can influence the UV absorption spectrum of a molecule. The HOMO of a molecule acts as an electron donor, while the LUMO accepts electrons. The spatial distribution and shape of these orbitals play a crucial role in determining the strength and orientation of electronic transitions that occur when the molecule absorbs UV radiation.[61]

The compounds studied are depicted in Figure 6, which displays the frontier orbitals and electrostatic potential maps. **5a** and **4** exhibit similar behavior, with boundary orbitals dispersed throughout the molecular structure. Conversely, **5b** displays a highly localized HOMO in the amino group, while its LUMO exhibits a distribution similar to that of the other compounds. Notably, the presence of dimethoxy groups significantly impacts electron fluxes, as indicated by the shape of the frontier orbitals. The absence of dimethoxy groups in the HOMO and LUMO orbitals suggests that they function as attractors rather than acceptors in the electron push−pull systems, confirming the explanation above based on bond distances. In addition, molecules with a HOMO localized in a donor group and a LUMO mainly localized in an acceptor group will have a strong absorption band at a wavelength corresponding to the energy difference between these orbitals. This happens because the transition from the HOMO to the LUMO is favorable and can be easily excited by UV radiation.[62−64]

Conversely, when a molecule's HOMO and LUMO are distributed throughout the molecule, the energy gap between them may be narrow, leading to a wide absorption spectrum, as shown in Figure 1. Moreover, as the solvent polarity increases, the emission spectra broaden. This is due to the stabilization of HOMO−LUMO transitions by the solvent's polarity, which promotes electronic transitions.[65]

Table 3 shows the absorption excitation energy, wavelengths of the lowest electronic transitions, and oscillator strengths for all compounds in THF. In all cases, the maximum oscillation
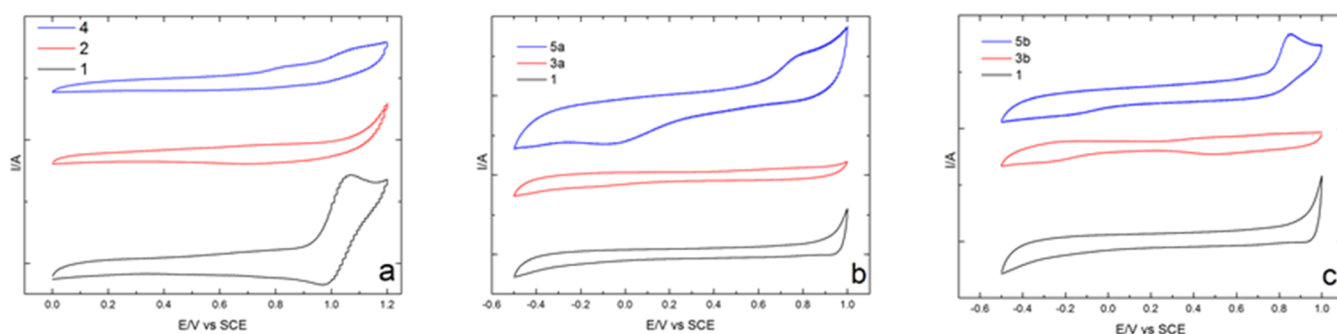
**Figure 7.** Cyclic voltammograms of the compounds (a) **4**, (b) **5a**, (c) **5b** and their precursors (**1**, **2**, **3a**, and **3b**) ($1.2 \times 10^{-2}$ M) in $CH_3CN$ with $1.2 \times 10^{-2}$ M $TBAPF_6$, $\nu = 100$ mV/s, $n = 5$.

**Table 4. Electrochemical Parameters Acquired from Voltammograms**

| compounds | $E_{onset,Oxi}$/V | $E_{onset,red}$/V | $E_{p, oxi}$/V | $E_{p, red}$/V | HOMO | LUMO | $E_g$/eV |
|---|---|---|---|---|---|---|---|
| **4$_{(1)}$** | 0.740 | | 0.819 | | 5.140 | | |
| **4$_{(2)}$** | 0.980 | 1.106 | 1.068 | 0.991 | 5.380 | 5.506 | 0.126 |
| **5a** | 0.638 | 0.975 | 0.778 | 0.864 | 5.038 | 5.375 | 0.337 |
| **5a$_2$** | | 0.240 | | −0.046 | | | |
| **5b** | 0.760 | 0.895 | 0.851 | 0.815 | 5.160 | 5.295 | 0.135 |
| **5b$_2$** | | −0.018 | | −0.191 | | | |

$E_{onset,Oxi}$: potential where the oxidation peak is initiated, $E_{onset,red}$: potential where the reduction peak is initiated, $E_p$: peak potential.

strength corresponds to the transition between the HOMO−LUMO orbitals, followed by the transition HOMO(−2)−LUMO(+2); these transitions are allowed due to the close in the shape of the orbital. Moreover, the occupied orbital was mainly localized in the aromatic ring. In contrast, the uncoupled orbital was centered on both the carbonyl and $\pi$ moiety, strongly suggesting an ICT process (carbonyl group) and, therefore, a $\pi-\pi^*$ transition. However, the presence of the dimethoxy group seems to break the donor process; computational calculations in this work suggest that the presence of two methoxy groups in the ring prevents resonance to the electron-accepting group. This behavior of the methoxy group has been reported before.[66]

The fluorescence efficiency is affected by the nature of a molecule's frontier orbitals. For example, Figure 5 shows that molecules with highly delocalized orbitals display stronger fluorescence due to the greater likelihood of the excited state electron returning to its ground state via radiative decay rather than nonradiative decay through alternative pathways like heat. Moreover, the shape of the frontier orbitals explains the behavior of the Stokes shift, which is the energy difference between a molecule's maximum absorption and maximum emission. Molecules with highly delocalized HOMO and LUMO experience a larger Stokes shift, resulting in a larger energy gap between excitation and emission. Nevertheless, a larger Stokes shift typically corresponds with a smaller quantum yield, as illustrated in Table 1.

**2.8. Electrochemical Studies.** Electrochemical redox behaviors (reduction and oxidation) of compounds **4**, **5a**, and **5b** and their precursors (**1**, **2**, **3a**, and **3b**) were investigated by cyclic voltammetry studies. All measures were obtained after finding the appropriate experimental conditions, such as applied potential range, scan rate ($\nu$), and the number of cycles ($n$). Figure 7 shows the voltammograms obtained at 100 mV/s for each compound of interest.

Compound **4** (see Figure 7a) shows two oxidation peaks, one at 0.819 V and the second at 1.068 V; possibly, these peaks

are due to the influence of precursors **2** and **1**, respectively. Precursor **2** shows an oxidation peak at 0.739 V, which could result from the oxidation of the OH attached to the aromatic ring,[67] while in **1**, it is observed at 1.068 V, which originated from the oxidation of the quinolone structure, the latter being an irreversible signal in terms of current obtained and peak potential difference.

Compounds **5a** and **5b** (see Figures 7b,7c) show much more marked and defined oxidation and reduction peaks than compound **4**. In Table 4, the peak potential values of each compound are detailed. Considering the voltammograms obtained for both compounds (**5a** and **5b**), it is possible to infer that the oxidation process is linked to the redox reaction of the segment coming from compound **1**; in both cases, it is observed that this signal is shown at lower peak potentials than in compound **4**, that is, less energy is required for the charge transfer to occur, which could indicate electrocatalysis of the reaction. The reduction processes observed at approximately −0.046 and −0.191 V for compounds **5a** and **5b**, respectively, are irreversible and may be linked to the reduction reaction of the segment of the molecule coming from the precursors **3a** and **3b**, respectively.

In certain investigations, the initiation of oxidation or reduction signals ($E_{onset,Oxi}$; $E_{onset,red}$) is utilized to estimate the energy levels of the highest occupied molecular orbital (HOMO) and lowest unoccupied molecular orbital (LUMO), respectively. This approach provides a means to quantify the electronic properties of molecules.[68] The results of these and other electrochemical parameters are listed in Table 4. The electrochemical $E_g$ values obtained are much lower than those estimated by spectroscopy; possibly, this difference is due to the influence of the solvent and the supporting electrolyte in the charge transfer process determined by cyclic voltammetry.[69]

**2.9. Cell Viability.** To determine the toxic effects of these compounds, the MTT assay was carried out using two prostate-cancer-derived cells and a normal cell line. The

cellular viability of the compounds **4**, **5a**, and **5b** was determined at different concentrations (60.0, 30.0, 15.0, 7.5, 3.8, 1.9 $\mu$M) to determine their 50% lethal concentration (LC$_{50}$) (Table 5 and Figure 8). Compound **5a** exhibited higher

**Table 5. *In Vitro* Antiproliferative Activity of Compounds 4 and 5a−b against a Normal Cell Line (BHK-21) and Two Prostate Cancer Cell Lines (LNCap and PC3)**

|  | compounds | | |
| --- | --- | --- | --- |
|  | 5a | 5b | 4 |
| cell line | LC$_{50}$ ($\mu$M) | | |
| BHK-21 | 49.70 | 36.00 | 8.10 |
| PC3 | 33.03 | 65.30 | >60 |
| LNCaP | 10.89 | 44.90 | >60 |

toxicity to tumor cells compared to the results obtained in BHK-21 cells, being 4.6 times more toxic to the LNCaP tumor line than normal cells. This is notably an advancement in the search for antitumor compounds or compounds useful in detecting cancer cells.

Motivated by the extraordinary fluorescence properties of compounds **4** and **5a−b**, we investigated their practical utility in live cell bioimaging and their efficient internalization in two human prostate cancer cells (LNCaP and PC3) and the normal cell BHk-21 (Figures 9−11). The results indicated the favorable cell permeability of compounds **4** and **5b**, along with their significant green fluorescence emission after excitation at 450−490 nm. Moreover, these compounds exhibited low-

intensity emission when excited at 365 nm, and no fluorescence emission was detected when cell cultures were excited at 575−625 nm and 460 nm. However, it is noteworthy that compounds **5b** and **4** uniquely emitted light at a wavelength of 520 nm exclusively in PC3 cells (Figure 11). This observation can be attributed to the distinctive traits of tumor cells. PC3, a prostate cancer cell line, is characterized by being poorly differentiated and androgen-independent, making it a highly aggressive form of cancer. This finding opens up possibilities for further exploration, as it could potentially serve as a marker for identifying tumor cells exhibiting aggressive phenotypes.

In general, prostate cancer cells, such as PC3 and LNCap, are characterized by high vesicular expression. This leads to the presence of characteristic multivesicular bodies, from which exosomes bud.[70] This characteristic is primarily observed in PC3 in Figure 11(A,E,I). Figure 11(B, F,J) demonstrates that the studied compounds can associate with these cellular structures because they exhibit a fluorescence with greater intensity, primarily composed of cytoplasmic proteins, such as actin, tubulin, and genetic material, including various RNA molecules.[71] It is noteworthy that both the nucleus and nucleolus, in all assays with different cell lines, exhibit much fainter fluorescence compared to the cytoplasm (Figures 9−11), suggesting that these compounds may not show affinity for nucleic acids but rather for various cytoplasmic proteins and different types of lipids. Additionally, when cells were excited at 450−490 nm, strong fluorescence was around the nuclei, suggesting an accumulation of the compound in the
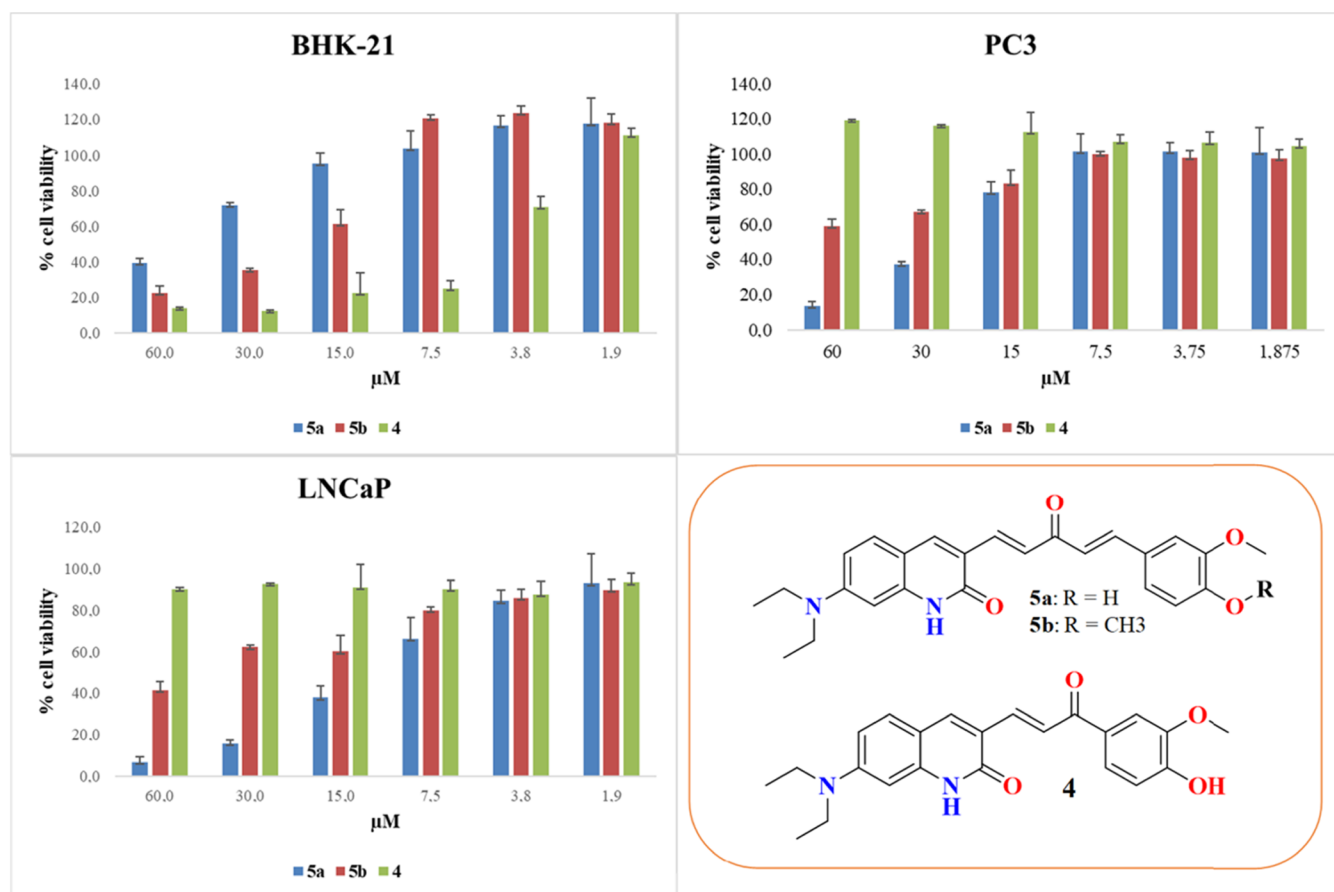


**Figure 8.** Cell viability of compounds **4** and **5a−b** against two human prostate cancer cells (LNCaP and PC3) and BHk-21 cell.
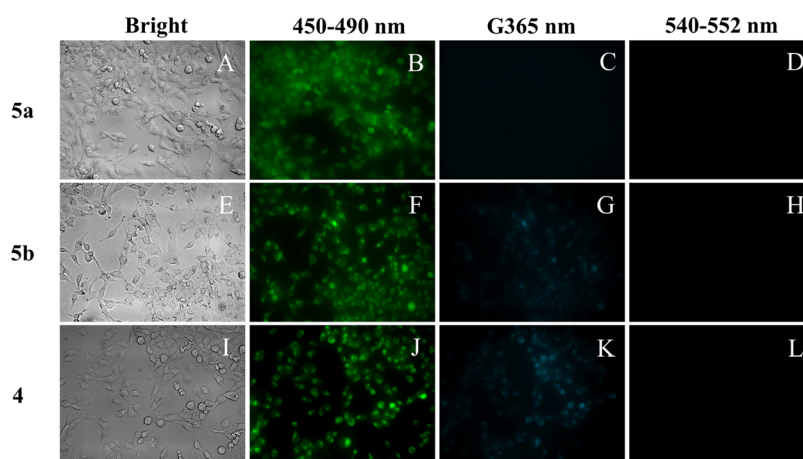
**Figure 9.** Microscopy fluorescence images of BHK-21 cells loaded with compound **4** (I−L) and compounds **5a** (A−D) and **5b** (E−H) excited at different wavelengths.
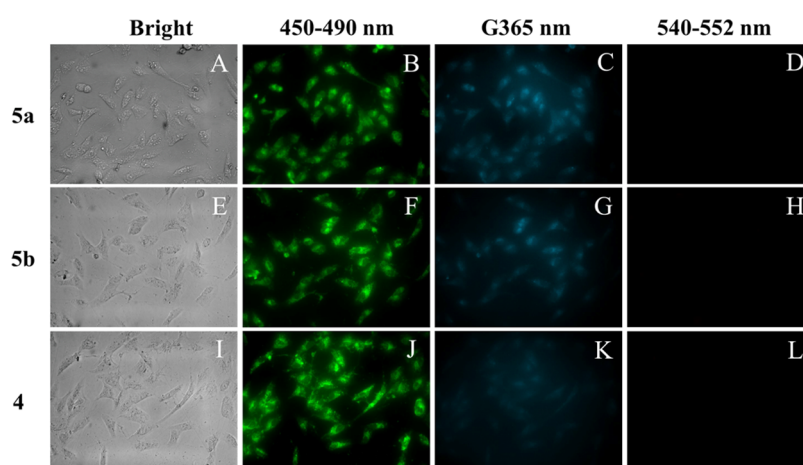


**Figure 10.** Microscopy fluorescence images of LNCaP cells loaded with compound **4** (I−L) and compounds **5a** (A−D) and **5b** (E−H) excited at different wavelengths.
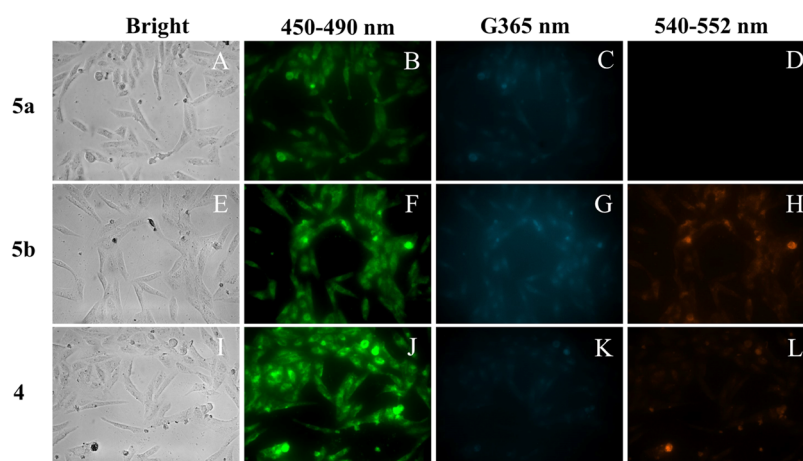


**Figure 11.** Microscopy fluorescence images of PC3 cells loaded with compound **4** (I−L) and compounds **5a** (A−D) and **5b** (E−H) excited at different wavelengths.

endoplasmic reticulum.[72,73] In this endomembrane system, lipid synthesis and modifications, as well as some protein synthesis, take place.[74] The potential association of the analyzed compounds with multivesicular bodies and the endoplasmic reticulum could be related to the slightly hydrophobic nature of these compounds, providing them with a certain selectivity when interacting with lipid or peptide cellular components. Future research on these compounds should focus on the mechanisms of action, cellular targets, and other potential effects, such as apoptosis activation, generation of reactive oxygen species, and genotoxic effects, among others.

## 3. CONCLUSIONS

In summary, we have synthesized three unsymmetrical 7-(diethylamino)quinolone chalcones with D-$\pi$-A-D and D-$\pi$-A-$\pi$-D type push–pull molecular arrangements via a Claisen–Schmidt reaction. The photophysical properties of compounds **4**, **5a**, and **5b** were studied. These dyes exhibited absorptions around 434–465 nm and emissions in the 502–606 nm range with considerable Stokes shifts caused by the ICT and TICT behavior. The general solvent effects in solvatofluorochromism were determined by the Reichardt ET, Lipper–Mataga, and Rettig plots that confirm the ICT and TICT process produced by the push–pull effect into D-$\pi$-A-D and D-$\pi$-A-$\pi$-D. The solid-state emission evidenced a red shift compared to the solution emission caused by the intermolecular $\pi$–$\pi$ interactions. The acid–base response shows the possible sites of protonation and deprotonation inside the molecules **4**, **5a**, and **5b**. Finally, all of these compounds exhibited a quenching behavior with the increase of $f_W$ caused by the typical TICT effect. The DFT results suggest that the compounds exhibit an intricate charge transfer within the D-$\pi$-A-D and D-$\pi$-A-$\pi$-D system, where the bonds involved in the charge transfer exhibit shorter lengths in the excited state, indicating an efficient electronic conjugation between the donor (D) and acceptor (A) groups. The obtained compounds showed moderate toxicity. However, compound **5a** exhibited 4.6 times higher toxicity on LNCaP than the normal cell line BHK-2. Furthermore, these fluorophores hold promising potential for utilization as cancer biomarkers.

## 4. EXPERIMENTAL SECTION

**4.1. Chemistry.** *4.1.1. General.* All organic chemicals and solvents were procured from Sigma-Aldrich, Fluka, AK Scientific, and Merck (analytical grade reagent) and used without further purification. IR spectra were recorded on a Shimadzu FTIR 8400 ATR spectrophotometer. Melting points were measured using a Stuart SMP3 melting point apparatus and are uncorrected. The 1H and 13C NMR spectra (400 MHz for proton and 100 MHz for carbon) were recorded on a Bruker Avance II 400 MHz NMR spectrometer, using DMSO-d6 (deuteration degree min. 99.95% for NMR spectroscopy MagniSolv) as the solvent and tetramethylsilane as an internal standard. Mass spectra were recorded on a SHIMADZU-GCMS 2010-DI-2010 spectrometer (equipped with a direct inlet probe) operating at 70 eV. TLC analyses were performed on silica gel aluminum plates (Merck 60 F254) and spots were visualized with ultraviolet irradiation.

*4.1.2. General Procedure for the Synthesis of bis 7-(Diethylamino)quinolone Chalcones.* 7-(diethylamino)-2-oxo-quinolinaldehyde **1** (1.0 mmol) was first dissolved in methanol (23 mL) and 5 mL of 10% KOH, and then ketones **2** and **3a–b** (1.0 mmol) were added. The reaction mixture was stirred for 36 h at room temperature. When the reaction finished, it was neutralized with HCl, and the resulting precipitate was collected by filtration, washed with MeOH/H₂O, and finally recrystallized from ethanol.

*4.1.2.1. 7-(Diethylamino)-3-((1E,4E)-5-(4-hydroxy-3-methoxyphenyl)-3-oxopenta-1,4-dien-1yl)quinolin-2(1H)-one (5a).* Red solid, mp 102–104 °C. FTIR (ATR) $\nu$ = [3363, 3168] (OH, NH), [1666, 1610] (C=O) cm⁻¹, ¹H NMR (400 MHz, DMSO-$d_6$) $\delta$ ppm: 11.47 (s, 1H), 8.19 (s, 1H), 7.67 (dd, $J$ = 11.3 Hz, 2H), 7.60 (d, $J$ = 15.7 Hz, 1H), 7.48 (d, $J$ = 9.0 Hz, 1H), 7.41 (s, 1H), 7.21 (d, $J$ = 8.0 Hz, 1H), 7.13 (d, $J$ = 15.8 Hz, 1H), 6.85 (d, $J$ = 8.1 Hz, 1H), 6.71 (d, $J$ = 9.2 Hz, 1H), 6.50 (s, 1H), 3.87 (s, 3H), 3.44 (q, 6.8 Hz, 4H), 1.16 (t, $J$ = 6.9 Hz, 6H). ¹³C NMR (101 MHz, DMSO-$d_6$) $\delta$ ppm: 188.3, 161.5, 150.3, 149.5, 148.0, 142.4, 141.7, 141.6, 138.8, 130.1, 126.3, 124.7, 123.5, 123.4, 119.0, 115.6, 111.3, 110.0, 109.0, 99.5, 93.8, 55.7, 44.2, 12.5. EI MS (70 eV): $m/z$ (%): 419 (M⁺: 5), 418 (17), 241 (100), 216 (9), 197 (13).

*4.1.2.2. 7-(Diethylamino)-3-((1E,4E)-5-(3,4-dimethoxyphenyl)-3-oxopenta-1,4-dien-1-yl)quinolin-2(1H)-one (5b).* Red solid, mp 83–85 °C $\nu$ = [3165] (NH), [1661] (C=O) cm⁻¹, ¹H NMR (400 MHz, DMSO-$d_6$) $\delta$ ppm: 8.15 (s, 1H), 7.74 (d, $J$ = 15.7 Hz, 1H), 7.68 (d, $J$ = 15.7 Hz, 1H), 7.62 (d, $J$ = 15.9 Hz, 1H), 7.45 (d, $J$ = 8.9 Hz, 1H), 7.44 (s, 1H), 7.32 (d, $J$ = 8.3 Hz, 1H), 7.21 (d, $J$ = 15.9 Hz, 1H), 7.03 (d, $J$ = 8.4 Hz, 1H), 6.67 (dd, $J$ = 9.0, 1.7 Hz, 1H), 6.50 (s, 1H), 3.86 (s, 3H), 3.83 (s, 3H), 3.42 (q, $J$ = 6.8 Hz, 4H), 1.15 (t, $J$ = 6.9 Hz, 6H). ¹³C NMR (101 MHz, DMSO) $\delta$ ppm: 188.9, 162.5, 151.5, 150.7, 149.5, 143.0, 142.4, 142.0, 139.9, 130.6, 128.2, 125.0, 124.9, 123.7, 119.4, 112.1, 110.9, 110.7, 109.4, 94.8, 56.1, 56.1, 44.6, 13.0. EI MS (70 eV): $m/z$ (%): 432 (M+: 9), 255 (67), 241 (100), 229 (21), 211 (15), 191 (23)

*4.1.2.3. (E)-7-(diethylamino)-3-(3-(4-hydroxy-3-methoxyphenyl)-3-oxoprop-1-en-1-yl)quinolin-2(1H)-one (4).* Orange solid, mp 100–101 °C. FTIR (ATR) $\nu$ = [3415, 3290] (OH, NH), [1647, 1610] (C=O) cm⁻¹, ¹H NMR (400 MHz, DMSO-$d_6$) $\delta$ ppm: 11.44 (s, 1H), 8.32 (s, 1H), 8.17 (d, $J$ = 15.4 Hz, 1H), 7.77 (d, $J$ = 15.4 Hz, 1H), 7.67 (d, $J$ = 8.0 Hz, 1H), 7.58 (s, 1H), 7.48 (d, $J$ = 9.0 Hz, 1H), 6.95 (d, $J$ = 8.2 Hz, 1H), 6.71 (d, $J$ = 8.6 Hz, 1H), 6.51 (s, 1H), 3.88 (s, 3H), 3.43 (q, $J$ = 6.2 Hz, 4H), 1.16 (t, $J$ = 6.8 Hz, 6H). ¹³C NMR (101 MHz, DMSO-$d_6$) $\delta$ ppm: 187.3, 161.6, 151.6, 150.3, 147.8, 141.7, 141.2, 139.3, 130.1, 130.1, 123.1, 120.1, 119.1, 115.0, 111.4, 110.0, 109.0, 93.9, 55.7, 44.2, 12.5, 12.4. EI MS (70 eV): $m/z$ (%): 392 (M+: 17), 241 (100), 197 (15) 151 (11),

**4.2. Computational Details.** The minimum energy surfaces of the compounds **4**, **5a**, and **5b** were determined using density functional theory (DFT) at the wb97xd/6-311g (d,p) level of theory.[75,76] The minimum energy structures were validated through frequency calculations, which ensured that all force constant values were greater than zero and verified that the minimum energy surface existed in all directions. Subsequently, electrostatic surface potential (ESP), frontier orbitals (HOMO and LUMO), and the excited state were computed by applying time-dependent density functional theory.[77]

*4.2.1. Theoretical Solvation Models.* The impact of the solvent on the behavior of the compounds described in the study was analyzed by using a polarized continuum solvation model based on density. The solvation model, which was implemented using G09 for Linux, was used to investigate the influence of the solvent on the compounds by incorporating the effect of solvent polarization into the calculations. The solvation model utilized the principles of the joint solvation model and the polarized continuum model, as described in the literature.[78,79] The goal of this study was to gain a deeper understanding of how the properties of the solvent impact the behavior of the compounds and to develop a more accurate and comprehensive model for predicting the behavior of similar compounds in different solvents. The results of this study are expected to provide important information for the design and optimization of new chemical compounds and to

advance our understanding of the complex interactions between solvents and solutes.

**4.3. Electrochemical Characterization.** Electrochemical experiments were carried out on an INTERFACE 1010E Gamry potentiostat−galvanostat and its respective Gamry Instruments Framework electrochemical research software suitable for computer control and recording of current−potential ($I$−$E$) curves. All experiments were carried out at room temperature and in an anchor-type electrochemical cell using a homemade Ag/AgCl electrode referenced with the saturated calomel electrode (SCE) as the reference electrode and a spiral-shaped platinum wire as the auxiliary electrode and as the working electrode, and in all cases, a platinum disk of 2 mm diameter was used. The electrolyte solution was prepared using tetrabutylammonium hexafluorophosphate for electrochemical analysis ≥99.0% as the supporting electrolyte and acetonitrile grade HPLC (Merck) as the solvent.

**4.4. Cytotoxicity Assays and Fluorescence Studies.** To analyze the behavior of compounds in cells, cytotoxicity assays and fluorescence studies were conducted in cell culture. Normal cells (BHK-21) and prostate cancer cells (PC3 and LNCaP) were used. All assays were carried out in RPMI 1640 medium, with 10% FBS and 2% penicillin−streptomycin at 37 °C with 5% $CO_2$ and complete humidity.[80,81]

To evaluate the cytotoxic effect of the compounds, the cell viability assay using the MTT reductase assay was employed, and $1 \times 10^4$ cells were seeded in each well of a 96-well plate and incubated for 24 h in RPMI 1640 medium with 10% FBS and 2% penicillin−streptomycin. After the cell adherence period, the wells were treated with different concentrations (60.0, 30.0, 15.0, 7.5, 3.8, 1.9 $\mu$M) of compounds (**4** and **5a**, **5b**). They were incubated for 24 h at 37 °C, 5% $CO_2$. Once the incubation time was completed, the medium was removed, and the wells were washed with PBS (pH: 7.4). A solution of MTT (0.5 mg/mL) diluted in serum-free RPMI was used. It was incubated again for 2−3 h to allow formazan formation. The medium was removed, and 100 $\mu$L of dimethyl sulfoxide (DMSO) was added to dissolve the formazan. Once it was completely dissolved, the absorbance was measured at a wavelength of 570 nm using a microplate reader (FLUOstar Omega). Data analysis was performed considering the negative control.[82,83] The fluorescence study was conducted using a motorized, inverted fluorescence microscope (Zeiss Axio-observer Z1) to visualize cells at 40× magnification, and images were captured using an Axiocam HRm. $5 \times 10^4$ cells were seeded in 24-well plates. Fifty thousand cells per well were grown in RPMI medium supplemented with 10% FBS and 2% penicillin−streptomycin at 37 °C and 5% $CO_2$. Subsequently, cell cultures were treated with the respective compound at 10 $\mu$M. Cells were imaged with a Zeiss Axio Observer Z1 motorized inverted fluorescence microscope at 40× magnification using the following filter cubes: FITC (set 10: excitation bandpass: 450−490 nm; emission bandpass: 515−565 nm), rhodamine (set 20: excitation bandpass: 546 ± 6 nm; emission bandpass: 575−640 nm), Cy5 (set 26: excitation bandpass: 575−625 nm; emission bandpass: 660−710 nm), DAPI (set 49: excitation: G365 nm; emission bandpass: 445 ± 25 nm), fields were selected, and images were taken for 5 and 15 min using a 40x objective and excitation channels at 488, 460, 520, and 660 nm.[84,85]

## ■ ASSOCIATED CONTENT

**Ⓢ Supporting Information**

The Supporting Information is available free of charge at https://pubs.acs.org/doi/10.1021/acsomega.3c07242.

> Absorption and emission normalized spectra of all compounds in a THF solution (S1), Lippert−Mataga and Rettig plots (S2). Emission spectra of **4**, **5a**, and **5b** in THF with TFA (S3) and TEA and ¹H NMR and ¹³C NMR spectra of all compounds (Figures S4−S6) (PDF)

## ■ AUTHOR INFORMATION

**Corresponding Author**

**Daniel Insuasty** − *Departamento de Química y Biología, División de Ciencias Básicas, Universidad del Norte, Puerto Colombia 081007, Colombia;* ⓞ orcid.org/0000-0001-9662-9505; Email: insuastyd@uninorte.edu.co

**Authors**

**Mario Mutis** − *Grupo de Investigación en Compuestos Heterocíclicos, Facultad de Ciencias Básicas, Universidad del Atlántico, Puerto Colombia 081007, Colombia*

**Jorge Trilleras** − *Grupo de Investigación en Compuestos Heterocíclicos, Facultad de Ciencias Básicas, Universidad del Atlántico, Puerto Colombia 081007, Colombia*

**Luis A. Illicachi** − *Grupo de Investigación en Química y Biotecnología, Facultad de Ciencias Básicas, Universidad Santiago de Cali, Cali 760032, Colombia*

**Juan D. Rodríguez** − *Programa de medicina, Facultad de Ciencias de la Salud, Universidad Libre, Puerto Colombia 081007, Colombia;* ⓞ orcid.org/0000-0001-5247-867X

**Andrea Ramos-Hernández** − *Grupo Química Supramolecular Aplicada, Semillero Electroquímica Aplicada, Facultad de Ciencias Básicas, Universidad del Atlántico, Puerto Colombia 081007, Colombia*

**Homero G. San-Juan-Vergara** − *Departamento de Medicina, División Ciencias de la Salud, Universidad del Norte, Puerto Colombia 081007, Colombia*

**Christian Cadena-Cruz** − *Departamento de Medicina, División Ciencias de la Salud, Universidad del Norte, Puerto Colombia 081007, Colombia*

**José R. Mora** − *Instituto de Simulación Computacional (ISC-USFQ), Departamento de Ingeniería Química, Universidad San Francisco de Quito, Quito 170901, Ecuador;* ⓞ orcid.org/0000-0001-6128-9504

**José L. Paz** − *Departamento Académico de Química Inorgánica, Facultad de Química e Ingeniería Química, Universidad Nacional Mayor de San Marcos, 15081 Lima, Perú;* ⓞ orcid.org/0000-0002-6177-7919

**Maximiliano Méndez-López** − *Departamento de Química y Biología, División de Ciencias Básicas, Universidad del Norte, Puerto Colombia 081007, Colombia;* ⓞ orcid.org/0000-0002-8919-2066

**Edwin G. Pérez** − *Organic Chemistry Department, Faculty of Chemistry and Pharmacy, Pontificia Universidad Católica de Chile, Santiago 7820436, Chile*

**Margarita E. Aliaga** − *Physical Chemistry Department, Faculty of Chemistry and Pharmacy, Pontificia Universidad Católica de Chile, Santiago 7820436, Chile*

**Jhesua Valencia** − *Departamento de Química y Biología, División de Ciencias Básicas, Universidad del Norte, Puerto Colombia 081007, Colombia*

**Edgar Márquez** − *Departamento de Química y Biología, División de Ciencias Básicas, Universidad del Norte, Puerto Colombia 081007, Colombia;* ● orcid.org/0000-0002-7503-1528

Complete contact information is available at:
https://pubs.acs.org/10.1021/acsomega.3c07242

**Notes**
The authors declare no competing financial interest.

## ■ REFERENCES

(1) Morin, J.-F. Recent Advances in the Chemistry of Vat Dyes for Organic Electronics. *J. Mater. Chem. C* **2017**, *5* (47), 12298−12307.

(2) Mustafa, C.; Ali Kemal, H.; Ender, A. Dye-Sensitized Solar Cell (DSSC) Applications Based on Cyano Functional Small Molecules Dyes. *Int. J. Opt. Photonic. Eng.* **2021**, *6* (2), 6 DOI: 10.35840/2631-5092/4540.

(3) Khalid, M.; Ali, A.; Jawaria, R.; Asghar, M. A.; Asim, S.; Khan, M. U.; Hussain, R.; Fayyaz ur Rehman, M.; Ennis, C. J.; Akram, M. S. First Principles Study of Electronic and Nonlinear Optical Properties of A−D−π−A and D−A−D−π−A Configured Compounds Containing Novel Quinoline−Carbazole Derivatives. *RSC Adv.* **2020**, *10* (37), 22273−22283.

(4) Sarder, P.; Maji, D.; Achilefu, S. Molecular Probes for Fluorescence Lifetime Imaging. *Bioconjugate Chem.* **2015**, *26* (6), 963−974.

(5) Mishra, S.; Kumar Singh, A. Real Time Sensor for $Fe^{3+}$, $Al^{3+}$, $Cu^{2+}$ & PPi through Quadruple Mechanistic Pathways Using a Novel Dipodal Quinoline-Based Molecular Probe. *Spectrochim. Acta, Part A* **2022**, *270*, No. 120832.

(6) Shi, Z.; Han, X.; Hu, W.; Bai, H.; Peng, B.; Ji, L.; Fan, Q.; Li, L.; Huang, W. Bioapplications of Small Molecule Aza-BODIPY: From Rational Structural Design to *in Vivo* Investigations. *Chem. Soc. Rev.* **2020**, *49* (21), 7533−7567.

(7) Chen, J.; Huang, D.; She, M.; Wang, Z.; Chen, X.; Liu, P.; Zhang, S.; Li, J. Recent Progress in Fluorescent Sensors for Drug-Induced Liver Injury Assessment. *ACS Sens.* **2021**, *6* (3), 628−640.

(8) Li, C.; Chen, G.; Zhang, Y.; Wu, F.; Wang, Q. Advanced Fluorescence Imaging Technology in the Near-Infrared-II Window for Biomedical Applications. *J. Am. Chem. Soc.* **2020**, *142* (35), 14789−14804.

(9) Meng, X.; Pang, X.; Zhang, K.; Gong, C.; Yang, J.; Dong, H.; Zhang, X. Recent Advances in Near-Infrared-II Fluorescence Imaging for Deep-Tissue Molecular Analysis and Cancer Diagnosis. *Small* **2022**, *18* (31), No. 2202035.

(10) Banerjee, S.; Veale, E. B.; Phelan, C. M.; Murphy, S. A.; Tocci, G. M.; Gillespie, L. J.; Frimannsson, D. O.; Kelly, J. M.; Gunnlaugsson, T. Recent Advances in the Development of 1,8-Naphthalimide Based DNA Targeting Binders, Anticancer and Fluorescent Cellular Imaging Agents. *Chem. Soc. Rev.* **2013**, *42* (4), 1601.

(11) Ferasat, E.; Golshan, M.; Salami-Kalajahi, M.; Roghani-Mamaqani, H. Synthesis and Properties of Fluorescent Coumarin/Perylene-3,4,9,10-Tetracarboxylic Diimide Hybrid as Cold Dye. *Mater. Res. Bull.* **2021**, *144*, No. 111500.

(12) Heynck, L.; Matthias, J.; Bossi, M. L.; Butkevich, A. N.; Hell, S. W. *N*-Cyanorhodamines: Cell-Permeant, Photostable and Bathochromically Shifted Analogues of Fluoresceins. *Chem. Sci.* **2022**, *13* (28), 8297−8306.

(13) Guo, R.; Yin, J.; Ma, Y.; Wang, Q.; Lin, W. A Novel Mitochondria-Targeted Rhodamine Analogue for the Detection of Viscosity Changes in Living Cells, Zebra Fish and Living Mice. *J. Mater. Chem. B* **2018**, *6* (18), 2894−2900.

(14) Aivali, S.; Tsimpouki, L.; Anastasopoulos, C.; Kallitsis, J. K. Synthesis and Optoelectronic Characterization of Perylene Diimide-Quinoline Based Small Molecules. *Molecules* **2019**, *24* (23), 4406.

(15) Shinde, S.; Sekar, N. Synthesis, Spectroscopic Characteristics, Dyeing Performance and TD-DFT Study of Quinolone Based Red Emitting Acid Azo Dyes. *Dyes Pigments* **2019**, *168*, 12−27.

(16) Dube, P. S.; Legoabe, L. J.; Beteck, R. M. Quinolone: A Versatile Therapeutic Compound Class. *Mol. Divers.* **2023**, *27*, 1501.

(17) Hu, Z.; Deng, Q.; Yang, S.; Guo, D. Preparation and Fluorescence Properties of Novel 2-Quinolone Derivatives and Their Corresponding Eu(III) Complexes. *Colloids Surf., A* **2020**, *599*, No. 124861.

(18) Lan, H.; Guo, T.; Dan, F.; Li, Y.; Tang, Q. Ratiometric Fluorescence Chemodosimeter for Hydrazine in Aqueous Solution and Gas Phase Based on Quinoline-Malononitrile. *Spectrochim. Acta, Part A* **2022**, *271*, No. 120892.

(19) Maltais, R.; Roy, J.; Poirier, D. Turning a Quinoline-Based Steroidal Anticancer Agent into Fluorescent Dye for Its Tracking by Cell Imaging. *ACS. Med. Chem. Lett.* **2021**, *12* (5), 822−826.

(20) Praveen Kumar, C. H.; Katagi, M. S.; Nandeshwarappa, B. P. Novel Synthesis of Quinoline Chalcone Derivatives - Design, Synthesis, Characterization and Antimicrobial Activity. *Chem. Data Collect.* **2022**, *42*, No. 100955.

(21) Sharma, S.; Singh, S. Synthetic Routes to Quinoline-Based Derivatives Having Potential Anti-Bacterial AndAnti-Fungal Properties. *Curr. Org. Chem.* **2022**, *26* (15), 1453−1469.

(22) Kaddah, M. M.; Morsy, A. R. I.; Fahmi, A. A.; Kamel, M. M.; Elsafty, M. M.; Rizk, S. A.; Ramadan, S. K. Synthesis and Biological Activity on IBD Virus of Diverse Heterocyclic Systems Derived from 2-Cyano- N '-((2-Oxo-1,2-Dihydroquinolin-3-Yl)Methylene)-Acetohydrazide. *Synth. Commun.* **2021**, *51* (22), 3366−3378.

(23) Radini, I.; Elsheikh, T.; El-Telbani, E.; Khidre, R. New Potential Antimalarial Agents: Design, Synthesis and Biological Evaluation of Some Novel Quinoline Derivatives as Antimalarial Agents. *Molecules* **2016**, *21* (7), 909.

(24) Valencia, J.; Rubio, V.; Puerto, G.; Vasquez, L.; Bernal, A.; Mora, J. R.; Cuesta, S. A.; Paz, J. L.; Insuasty, B.; Abonia, R.; Quiroga, J.; Insuasty, A.; Coneo, A.; Vidal, O.; Márquez, E.; Insuasty, D. QSAR Studies, Molecular Docking, Molecular Dynamics, Synthesis, and Biological Evaluation of Novel Quinolinone-Based Thiosemicarbazones against Mycobacterium Tuberculosis. *Antibiotics* **2023**, *12* (1), 61.

(25) Bacci, A.; Corsi, F.; Runfola, M.; Sestito, S.; Piano, I.; Manera, C.; Saccomanni, G.; Gargini, C.; Rapposelli, S. Design, Synthesis, and In Vitro Evaluation of Novel 8-Amino-Quinoline Combined with Natural Antioxidant Acids. *Pharmaceuticals* **2022**, *15* (6), 688.

(26) Mohamed, M. F. A.; Abuo-Rahma, G. E.-D. A. Molecular Targets and Anticancer Activity of Quinoline−Chalcone Hybrids: Literature Review. *RSC Adv.* **2020**, *10* (52), 31139−31155.

(27) Anizaim, A. H.; Zainuri, D. A.; Zaini, M. F.; Razak, I. A.; Bakhtiar, H.; Arshad, S. Comparative Analyses of New Donor-π-Acceptor Ferrocenyl-Chalcones Containing Fluoro and Methoxy-Fluoro Acceptor Units as Synthesized Dyes for Organic Solar Cell Material. *PLoS One* **2020**, *15* (11), No. e0241113.

(28) Kagatikar, S.; Sunil, D.; Kekuda, D.; Satyanarayana, M. N.; Kulkarni, S. D.; Sudhakar, Y. N.; Vatti, A. K.; Sadhanala, A. Pyrene-Based Chalcones as Functional Materials for Organic Electronics Application. *Mater. Chem. Phys.* **2023**, *293*, No. 126839.

(29) Sachdeva, T.; Milton, M. D. AIEE Active Novel Red-Emitting D-π-A Phenothiazine Chalcones Displaying Large Stokes Shift, Solvatochromism and "Turn-on" Reversible Mechanofluorochromism. *Dyes Pigments* **2020**, *181*, No. 108539.

(30) Batista, A. S.; Oliveira, S. D. S.; Pomel, S.; Commere, P.-H.; Mazan, V.; Lee, M.; Loiseau, P. M.; Rossi-Bergmann, B.; Prina, E.; Duval, R. Targeting Chalcone Binding Sites in Living Leishmania

Using a Reversible Fluorogenic Benzochalcone Probe. *Biomed. Pharmacother.* 2022, *149*, No. 112784.

(31) Yildirim, B.; Beşer, B. M.; ÇOlak, N. U.; Altay, A.; Yaşar, A. Fluorescence Interactions of a Novel Chalcone Derivative with Membrane Model Systems and Human Serum Albumin. *Biophys. Chem.* 2022, *290*, No. 106879.

(32) Allott, L.; Brickute, D.; Chen, C.; Braga, M.; Barnes, C.; Wang, N.; Aboagye, E. O. Development of a Fluorine-18 Radiolabelled Fluorescent Chalcone: Evaluated for Detecting Glycogen. *EJNMMI Radiopharm. Chem.* 2020, *5* (1), 17.

(33) Insuasty, D.; García, S.; Abonia, R.; Insuasty, B.; Quiroga, J.; Nogueras, M.; Cobo, J.; Borosky, G. L.; Laali, K. K. Design, Synthesis, and Molecular Docking Study of Novel Quinoline-based Bis-chalcones as Potential Antitumor Agents. *Arch. Pharm.* 2021, *354* (9), No. 2100094.

(34) Insuasty, D.; Cabrera, L.; Ortiz, A.; Insuasty, B.; Quiroga, J.; Abonia, R. Synthesis, Photophysical Properties and Theoretical Studies of New Bis-Quinolin Curcuminoid BF2-Complexes and Their Decomplexed Derivatives. *Spectrochim. Acta, Part A* 2020, *230*, No. 118065.

(35) Reichardt, C. W. T. Solvent Effects on the Absorption Spectra of Organic Compounds. In *Solvents and Solvent Effects in Organic Chemistry*; Wiley-VCH Verlag GmbH & Co. KGaA: Weinheim, Germany, 2010; pp 359−424.

(36) Singh, V. D.; Kushwaha, A. K.; Singh, R. S. Achieving Flexibility/Rigidity Balance through Asymmetric Donor−Acceptor Scaffolds in Pursuit of Dual State Emission with Application in Acidochromism. *Dyes Pigments* 2021, *187*, No. 109117.

(37) Chen, H.; Fang, S.; Wang, L.; Liu, X.; Yan, J.; Zhang, N.; Zheng, K. Tetraphenylene-Chalcone Hybrid Derivatives: Synthesis, Structural, Fluorescence Properties and Imaging in Living Cells. *J. Mol. Liq.* 2021, *321*, No. 114913.

(38) Grabowski, Z. R.; Rotkiewicz, K.; Rettig, W. Structural Changes Accompanying Intramolecular Electron Transfer: Focus on Twisted Intramolecular Charge-Transfer States and Structures. *Chem. Rev.* 2003, *103* (10), 3899−4032.

(39) El-Zohry, A. M.; Orabi, E. A.; Karlsson, M.; Zietz, B. Twisted Intramolecular Charge Transfer (TICT) Controlled by Dimerization: An Overlooked Piece of the TICT Puzzle. *J. Phys. Chem. A* 2021, *125* (14), 2885−2894.

(40) Chen, J.; Xu, Z.; Zheng, J.; Wu, H.; Chi, Y. Phototriggered Color Modulation of Perovskite Nanoparticles for High Density Optical Data Storage. *Chem. Sci.* 2022, *13* (35), 10315−10326.

(41) Liu, Y.-H.; Lan, S.-C.; Zhu, C.; Lin, S.-H. Intersystem Crossing Pathway in Quinoline−Pyrazole Isomerism: A Time-Dependent Density Functional Theory Study on Excited-State Intramolecular Proton Transfer. *J. Phys. Chem. A* 2015, *119* (24), 6269−6274.

(42) Wang, C.; Qiao, Q.; Chi, W.; Chen, J.; Liu, W.; Tan, D.; McKechnie, S.; Lyu, D.; Jiang, X.-F.; Zhou, W.; Xu, N.; Zhang, Q.; Xu, Z.; Liu, X. Quantitative Design of Bright Fluorophores and AIEgens by the Accurate Prediction of Twisted Intramolecular Charge Transfer (TICT). *Angew. Chem., Int. Ed.* 2020, *59* (25), 10160−10172.

(43) Reichardt, C. Solvatochromic Dyes as Solvent Polarity Indicators. *Chem. Rev.* 1994, *94* (8), 2319−2358.

(44) Kucherak, O. A.; Didier, P.; Mély, Y.; Klymchenko, A. S. Fluorene Analogues of Prodan with Superior Fluorescence Brightness and Solvatochromism. *J. Phys. Chem. Lett.* 2010, *1* (3), 616−620.

(45) Ibrahim Mohamed Allaoui, Z.; le Gall, E.; Fihey, A.; Plaza-Pedroche, R.; Katan, C.; Robin-le Guen, F.; Rodríguez-López, J.; Achelle, S. Push−Pull (Iso)Quinoline Chromophores: Synthesis, Photophysical Properties, and Use for White-Light Emission. *Eur. J. Chem.* 2020, *26* (36), 8153−8161.

(46) Lippert, E. Spektroskopische Bestimmung Des Dipolmomentes Aromatischer Verbindungen Im Ersten Angeregten Singulettzustand. *Z. Elektrochem., Berichte Bunsengesellschaft Phys. Chem.* 1957, *61*, 962−975.

(47) Prusti, B.; Chakravarty, M. Electron-Rich Anthracene-Based Twisted π-System as a Highly Fluorescent Dye: Easy Recognition of

(48) *Solvent and Environmental Effects BT - Principles of Fluorescence Spectroscopy*; Lakowicz, J. R., Ed.; Springer US: Boston, MA, 2006; pp 205−235.

(49) Sachdeva, T.; Milton, M. D. AIEE Active Novel Red-Emitting D-π-A Phenothiazine Chalcones Displaying Large Stokes Shift, Solvatochromism and "Turn-on" Reversible Mechanofluorochromism. *Dyes Pigm.* 2020, *181*, No. 108539.

(50) Khopkar, S.; Jachak, M.; Shankarling, G. Viscosity Sensitive Semisquaraines Based on 1, 1, 2-Trimethyl-1H-Benzo[e]Indole: Photophysical Properties, Intramolecular Charge Transfer, Solvatochromism, Electrochemical and DFT Study. *J. Mol. Liq.* 2019, *285*, 123−135.

(51) Sachdeva, T.; Milton, M. D. AIEE Active Novel Red-Emitting D-π-A Phenothiazine Chalcones Displaying Large Stokes Shift, Solvatochromism and "Turn-on" Reversible Mechanofluorochromism. *Dyes Pigments* 2020, *181*, No. 108539.

(52) Zhu, H.; Zhang, S.; Yang, J.; Wu, M.; Wu, Q.; Liu, J.; Zhang, J.; Kong, L.; Yang, J. Tunable Aggregation-Induced Emission, Solid-State Fluorescence, and Mechanochromic Behaviors of Tetraphenylethene-Based Luminophores by Slight Modulation of Substituent Structure. *J. Solid State Chem.* 2022, *305*, No. 122706.

(53) Khopkar, S.; Jachak, M.; Shankarling, G. Viscosity Sensitive Semisquaraines Based on 1,1, 2-Trimethyl-1H-Benzo[e]indole: Photophysical Properties, Intramolecular Charge Transfer, Solvatochromism, Electrochemical and DFT Study. *J. Mol. Liq.* 2019, *285*, 123−135.

(54) de França, B. M.; Oliveira, S. S. C.; Souza, L. O. P.; Mello, T. P.; Santos, A. L. S.; Bello Forero, J. S. Synthesis and Photophysical Properties of Metal Complexes of Curcumin Dyes: Solvatochromism, Acidochromism, and Photoactivity. *Dyes Pigments* 2022, *198*, No. 110011.

(55) Liu, H.; Cao, Y.; Deng, Y.; Wei, L.; Yan, J.; Xiao, L. Enhanced β-Amyloid Aggregation in Living Cells Imaged with Quinolinium-Based Spontaneous Blinking Fluorophores *Chem. Biomed. Imaging* 2023, DOI: 10.1021/cbmi.3c00081.

(56) Liu, X.; Qiao, Q.; Tian, W.; Liu, W.; Chen, J.; Lang, M. J.; Xu, Z. Aziridinyl Fluorophores Demonstrate Bright Fluorescence and Superior Photostability by Effectively Inhibiting Twisted Intramolecular Charge Transfer. *J. Am. Chem. Soc.* 2016, *138* (22), 6960−6963.

(57) Sasaki, S.; Suzuki, S.; Sameera, W. M. C.; Igawa, K.; Morokuma, K.; Konishi, G. Highly Twisted N,N-Dialkylamines as a Design Strategy to Tune Simple Aromatic Hydrocarbons as Steric Environment-Sensitive Fluorophores. *J. Am. Chem. Soc.* 2016, *138* (26), 8194−8206.

(58) Shen, X. Y.; Yuan, W. Z.; Liu, Y.; Zhao, Q.; Lu, P.; Ma, Y.; Williams, I. D.; Qin, A.; Sun, J. Z.; Tang, B. Z. Fumaronitrile-Based Fluorogen: Red to near-Infrared Fluorescence, Aggregation-Induced Emission, Solvatochromism, and Twisted Intramolecular Charge Transfer. *J. Phys. Chem. C* 2012, *116* (19), 10541−10547.

(59) Song, X.-M.; Feng, Z.-C.; Wu, Y.; Song, J.-L.; Wei, L.-F.; Zeng, S.-Y. Triphenylamine-Based Conjugated Fluorescent Sensor for Highly Sensitive Detection of Water in Organic Solvents. *J. Mol. Liq.* 2022, *365*, No. 120086.

(60) Jayabharathi, J.; Thanikachalam, V.; Srinivasan, N.; Venkatesh Perumal, M. Fluorescence Spectral Studies of Some Imidazole Derivatives. *Spectrochim. Acta, Part A* 2012, *90*, 125−130.

(61) Krishnan, S.; Senthilkumar, K. The Influence of the Shape and Configuration of Sensitizer Molecules on the Efficiency of DSSCs: A Theoretical Insight. *RSC Adv.* 2021, *11* (10), 5556−5567.

(62) Narsaria, A. K.; Poater, J.; Fonseca Guerra, C.; Ehlers, A. W.; Lammertsma, K.; Bickelhaupt, F. M. Rational Design of Near-Infrared Absorbing Organic Dyes: Controlling the HOMO-LUMO Gap Using Quantitative Molecular Orbital Theory. *J. Comput. Chem.* 2018, *39* (32), 2690−2696.

(63) Lv, X.; Li, Z.; Li, S.; Luan, G.; Liang, D.; Tang, S.; Jin, R. Design of Acceptors with Suitable Frontier Molecular Orbitals to

Match Donors via Substitutions on Perylene Diimide for Organic Solar Cells. *Int. J. Mol. Sci.* **2016**, *17* (5), 721.

(64) El Kouari, Y.; Migalska-Zalas, A.; Arof, A. K.; Sahraoui, B. Computations of Absorption Spectra and Nonlinear Optical Properties of Molecules Based on Anthocyanidin Structure. *Opt. Quantum Electron* **2015**, *47* (5), 1091−1099.

(65) Más-Montoya, M.; García Alcaraz, A.; Espinosa Ferao, A.; Bautista, D.; Curiel, D. Insight into the Stokes Shift, Divergent Solvatochromism and Aggregation-Induced Emission of Boron Complexes with Locked and Unlocked Benzophenanthridine Ligands. *Dyes Pigments* **2023**, *209*, No. 110924.

(66) Wazzan, N.; Safi, Z. Effect of Number and Position of Methoxy Substituents on Fine-Tuning the Electronic Structures and Photophysical Properties of Designed Carbazole-Based Hole-Transporting Materials for Perovskite Solar Cells: DFT Calculations. *Arab. J. Chem.* **2019**, *12* (1), 1−20.

(67) Zhou, Q.; Zhai, H. Y.; Pan, Y. F.; Li, K. A Simple and Sensitive Sensor Based on a Molecularly Imprinted Polymer-Modified Carbon Paste Electrode for the Determination of Curcumin in Foods. *RSC Adv.* **2017**, *7* (37), 22913−22918.

(68) Cardona, C. M.; Li, W.; Kaifer, A. E.; Stockdale, D.; Bazan, G. C. Electrochemical Considerations for Determining Absolute Frontier Orbital Energy Levels of Conjugated Polymers for Solar Cell Applications. *Adv. Mater.* **2011**, *23* (20), 2367−2371.

(69) Wang, D.; Yao, Q.; Shao, T.; Wang, Z.; Ma, Y.; Wang, C. Thiophene or Pyridine-Substituted Quinoline Derivatives: Synthesis, Properties, and Electropolymerization for Energy Storage. *Int. J. Energy. Res.* **2023**, *2023*, 4726892.

(70) Vlaeminck-Guillem, V. Extracellular Vesicles in Prostate Cancer Carcinogenesis, Diagnosis, and Management. *Front. Oncol.* **2018**, *8* (JUN), 1.

(71) Xu, M.; Ji, J.; Jin, D.; Wu, Y.; Wu, T.; Lin, R.; Zhu, S.; Jiang, F.; Ji, Y.; Bao, B.; Li, M.; Xu, W.; Xiao, M. The Biogenesis and Secretion of Exosomes and Multivesicular Bodies (MVBs): Intercellular Shuttles and Implications in Human Diseases. *Genes Dis.* **2023**, *10*, 1894.

(72) Zang, S.; Kong, X.; Cui, J.; Su, S.; Shu, W.; Jing, J.; Zhang, X. Revealing the Redox Status in Endoplasmic Reticulum by a Selenium Fluorescence Probe. *J. Mater. Chem. B* **2020**, *8* (13), 2660−2665.

(73) Shu, W.; Zang, S.; Wang, C.; Gao, M.; Jing, J.; Zhang, X. An Endoplasmic Reticulum-Targeted Ratiometric Fluorescent Probe for the Sensing of Hydrogen Sulfide in Living Cells and Zebrafish. *Anal. Chem.* **2020**, *92* (14), 9982−9988.

(74) Qi, Z.; Chen, L. Endoplasmic Reticulum Stress and Autophagy. *Adv. Exp. Med. Biol.* **2019**, *1206*, 167−177.

(75) Parr, R. G. Density Functional Theory. *Annu. Rev. Phys. Chem.* **1983**, *34* (1), 631−656.

(76) Chai, J.-D.; Head-Gordon, M. Long-Range Corrected Hybrid Density Functionals with Damped Atom−Atom Dispersion Corrections. *Phys. Chem. Chem. Phys.* **2008**, *10* (44), 6615.

(77) Burke, K.; Werschnik, J.; Gross, E. K. U. Time-Dependent Density Functional Theory: Past, Present, and Future. *J. Chem. Phys.* **2005**, *123* (6), 062206.

(78) Mennucci, B. Polarizable Continuum Model. *WIREs Comput. Mol. Sci.* **2012**, *2* (3), 386−404.

(79) Marenich, A. V.; Cramer, C. J.; Truhlar, D. G. Universal Solvation Model Based on Solute Electron Density and on a Continuum Model of the Solvent Defined by the Bulk Dielectric Constant and Atomic Surface Tensions. *J. Phys. Chem. B* **2009**, *113* (18), 6378−6396.

(80) Sher, N.; Ahmed, M.; Mushtaq, N.; Khan, R. A. Cytotoxicity and Genotoxicity of Green Synthesized Silver, Gold, and Silver/Gold Bimetallic NPs on BHK-21 Cells and Human Blood Lymphocytes Using MTT and Comet Assay. *Appl. Organomet. Chem.* **2023**, *37* (2), No. e6968.

(81) Kudic, B. Corrigendum: IC50: An Unsuitable Measure for Large-Sized Prostate Cancer Spheroids in Drug Sensitivity Evaluation. *Biomol. Biomed.* **2023**, *23* (3), 545.

(82) Satari, A.; Amini, S. A.; Raeisi, E.; Lemoigne, Y.; Hiedarian, E. Synergetic Impact of Combined 5-Fluorouracil and Rutin on Apoptosis in PC3 Cancer Cells through the Modulation of P53 Gene Expression. *Adv. Pharm. Bull.* **2019**, *9* (3), 462−469.

(83) Ghasemi, M.; Turnbull, T.; Sebastian, S.; Kempson, I. The Mtt Assay: Utility, Limitations, Pitfalls, and Interpretation in Bulk and Single-Cell Analysis. *Int. J. Mol. Sci.* **2021**, *22* (23), 12827 DOI: 10.3390/ijms222312827.

(84) Singh, A. K.; Singh, V. K.; Singh, M.; Singh, P.; Khadim, S. R.; Singh, U.; Koch, B.; Hasan, S. H.; Asthana, R. K. One Pot Hydrothermal Synthesis of Fluorescent NP-Carbon Dots Derived from Dunaliella Salina Biomass and Its Application in on-off Sensing of Hg (II), Cr (VI) and Live Cell Imaging. *J. Photochem. Photobiol., A* **2019**, *376*, 63−72.

(85) Eskalen, H.; Uruş, S.; Cömertpay, S.; Kurt, A. H.; Özgan, Ş. Microwave-Assisted Ultra-Fast Synthesis of Carbon Quantum Dots from Linter: Fluorescence Cancer Imaging and Human Cell Growth Inhibition Properties. *Ind. Crops. Prod.* **2020**, *147*, No. 112209.